Available online at www.sciencedirect.com
SCIENCE DIRECT®
Journal of Computational Physics 199 (2004) 437–464
JOURNAL OF COMPUTATIONAL PHYSICS
www.elsevier.com/locate/jcp

Two-component plasma model for two-dimensional glow discharge in magnetic field

Sergey T. Surzhikov, Joseph S. Shang *

Institute for Problems in Mechanics Russian Academy of Sciences, Moscow Wright State University, Dayton, OH 45435-0001, USA

Received 23 July 2003; received in revised form 2 February 2004; accepted 2 February 2004
Available online 2 April 2004

Abstract

Theory and computational model for a glow discharge in a parallel-plate configuration with an applied transversal magnetic field is presented. The model is based on the diffusion-drift theory of gas discharge consisting of continuity and momentum conservation equations for electron and ion fluids, as well as the Poisson equation for the self-consistent electric field. Two-dimensional numerical results are obtained for nitrogen at a pressure range from 5 to 10 torr, the electromotive force of power supply of 2–3 kV, and magnetic field induction of $-0.1 \leqslant B \leqslant 0.1$ T. The present results, without the applied external magnetic field, compare favorably with the classic theory of von Engel and Steenbeck. For the first time, the physics-based model also successfully applies to the glow discharge under the influence of an external magnetic field. It has been shown that at $B \sim 0.01$ T, the glow discharge shifts correctly in the normal direction relative to both the magnetic and electric fields.

1. Introduction

Achievements in aerospace and electromagnetic technologies of past decades allow a real possibility to create hypersonic air vehicles at a Mach number greater than 6. At such high velocity, the traditional flow control mechanism is often ineffective due to significant physical–chemical modification of airflow. Under this condition, additional physical mechanisms for flow control become necessary. Since the later 1950s, scientific literature has discussed the possibilities of using electromagnetic fields for modifying weakly ionizing gas flows in aerospace applications [1,2]. A productive approach to flow control can be derived from applying an external electromagnetic force to a flow field in an electrically conducting medium.

One of the well-known physical methods for enhancing the electrical conductivity of the flow medium is using glow discharge (see Fig. 1). This type of electrical discharges is widely used in plasma generation for physical investigations due to its simplicity and high efficiency. However, even for this relative simple plasma generation process, there is very limited numerical simulation capability to describe the glow

* Corresponding author. Tel.: +1-937-775-5094.
E-mail address: jshang@cs.wright.edu (J.S. Shang).

0021-9991/$ - see front matter © 2004 Elsevier Inc. All rights reserved.
doi:10.1016/j.jcp.2004.02.019

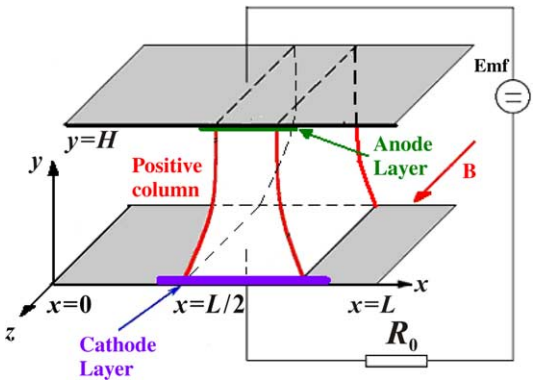

Fig. 1. Schematic of a glow discharge with external magnetic field.

discharge behavior. The pioneering efforts by Engel and Steenbeck [3,4], Brown [5], Howatson [6], and Raizer [7] in the physics of gas discharge are well known, their mathematic models were built on the dominant physical process of the forced diffusion and drift velocity of charged particles. This predictive theory has demonstrated a wide range of applicability of the fully ionized gas mixture. However, a challenging issue of the diffusion-drift model is encountered in the sheath region of the electrodes where the charge separation takes place to drastically alter the physical behavior of the discharge column [7,8]. Through the works of Ward [9,10], Graves and Jensen [11], Boeuf and Marode [12], and Raizer and Surzhikov [13,14], it was found that the diffusion-drift model has a validated range beyond expectation. Incorporating the physics-based approximate boundary conditions indeed may extend the applicability of the diffusion-drift model.

In glow discharge, the main supply of electrons is obtained from the secondary emission from the cathode by the impingement of the positive ions [3–6]. The energy exchanged in collision for a weakly ionized gas can still be purely kinetic. In other words, the electromagnetic forces between charged particles can only produce a negligible path deflection at considerable distance. The physics becomes increasingly complex when the glow discharge is subjected to an external magnetic field, because charged particles tend to gyrate around the lines of magnetic flux. This interaction with the magnetic field affects the drift velocity generated by electrical field and concentration gradient.

In aerospace application, the magnetic Reynolds number of the glow discharge is often negligible, thus the induced magnetic field is also insignificant [1–5]. To achieve a strong electromagnetic-aerodynamic interaction, plasma generation by glow discharge is frequently applied concurrently with an external magnetic field. Therefore, a better understanding and the ability to model the effect of an applied external magnetic field is essential.

The main subject of the present study is focused on the interaction of a glow discharge with external magnetic field, which are of practical interest for aerospace applications. Based on the developed theory of glow discharges in magnetic field, it will be shown that the magnetic field can be used as control mechanism for modifying physical structure of the glow discharge.

2. Diffusion-drift model of glow discharge

Direct current glow discharges (DCGD) are weakly ionized gases sustained by an external electric field. The applied field, coupled with the relatively low rate of energy transfer between electrons and the much more massive neutral species, results in highly energetic electrons (electron temperature $T_e > 10,000$ K and relatively low temperature neutral species ($T_n \sim 300$ K). Ions transfer energy readily in elastic collisions

with neutral species and are therefore usually near the neutral species temperature. Because of the huge difference in energy contents of electron and neutral species, the discharge is not in thermodynamic equilibrium. Furthermore, the highly energetic electrons are capable of ionizing and dissociating the neutral species at high rate even though the bulk gas temperature is quite low.

It was found that a diffusion-drift model of partially ionized gas mixture (neutrals, ions and electrons) can predict all general characteristics of such discharges in the pressure range from 1 to 50 torr and with voltage drops across the electrodes from 0.3 to 10 kV [7,9–11,13,14]. Taking into account the fact that a glow discharge is a weekly ionizing gas, it is possible to include the undisturbed external magnetic field. This implement will affect the electrodynamic structure of the glow discharge, but will not significantly disturb the plasma generation process. A mathematic model of this phenomenon will also be investigated by the present effort.

A planar glow discharge in molecular nitrogen between flat electrodes is considered (Fig. 1). The diffusion-drift theory [3,7,9,11] will be used for description of gas discharge processes. This theory is based on continuity equations for concentration of electrons n_e and positive ions n_+ together with the equations for the electro-static field $\mathbf{E} = -\operatorname{grad}\varphi$:

$$\frac{\partial n_e}{\partial t} + \frac{\partial \Gamma_{e,x}}{\partial x} + \frac{\partial \Gamma_{e,y}}{\partial y} = \alpha(E,p)|\Gamma_e| - \beta n_+ n_e, \tag{1}$$

$$\frac{\partial n_+}{\partial t} + \frac{\partial \Gamma_{+,x}}{\partial x} + \frac{\partial \Gamma_{+,y}}{\partial y} = \alpha(E,p)|\Gamma_e| - \beta n_+ n_e, \tag{2}$$

$$\frac{\partial^2 \varphi}{\partial x^2} + \frac{\partial^2 \varphi}{\partial y^2} = 4\pi e(n_e - n_+), \tag{3}$$

where Γ_e and Γ_i are the electron and ion flux densities, respectively,

$$\Gamma_e = -D_e \operatorname{grad} n_e - n_e \mu_e \mathbf{E}, \Gamma_+ = -D_+ \operatorname{grad} n_+ + n_+ \mu_+ \mathbf{E}.$$

In this formulation, $\alpha(E,p)$ and β are the first Townsend ionization coefficient and recombination coefficient, μ_e and μ_+ are the electron and ion mobilities, and D_e and D_+ are the electron and ion diffusion coefficients. In the charge conservation equation (3), φ is the potential of electric field, and the e is the electron charge, $e = 1.6 \times 10^{-19}$ C. As it will be discussed later, $\mathbf{j}$ is the electric current density, $\mathbf{j} = e(\Gamma_+ - \Gamma_e), |\Gamma_e| = \sqrt{\Gamma_{e,x}^2 + \Gamma_{e,y}^2}$.

To introduce a magnetic field in the model, the following momentum conservation equations for electronic and ionic particles must be included [8,15]:

$$\rho_e \frac{\partial \mathbf{u}_e}{\partial t} + \rho_e(\mathbf{u}_e \cdot \nabla)\mathbf{u}_e = -\nabla p_e - \tau_e - e n_e \left(\mathbf{E} + \frac{1}{c}[\mathbf{u}_e \mathbf{B}]\right) - m_e \nu_{en} n_e(\mathbf{u}_e - \mathbf{u}_n) - m_e \nu_{e+} n_e(\mathbf{u}_e - \mathbf{u}_+), \tag{4}$$

$$\rho_+ \frac{\partial \mathbf{u}_+}{\partial t} + \rho_+(\mathbf{u}_+ \cdot \nabla)\mathbf{u}_+ = -\nabla p_+ - \tau_+ + e n_+ \left(\mathbf{E} + \frac{1}{c}[\mathbf{u}_+ \mathbf{B}]\right) - m_+ \nu_{+e} n_i(\mathbf{u}_+ - \mathbf{u}_e) - m_+ \nu_{+n} n_+(\mathbf{u}_+ - \mathbf{u}_n), \tag{5}$$

where $\mathbf{u}_e, \mathbf{u}_+$ are the velocities of electronic and ionic gases, ρ_e, ρ_+ are the densities of electronic and ionic gases, $\rho_e = m_e n_e$, $\rho_+ = m_+ n_+$, m_e, m_+ are the mass of electron and ion. The $\mathbf{u}_n$ is the mass-averaged velocity of neutral particles, p_e, p_+ are the electronic and ionic pressures, τ_e, τ_+ are the viscosity stress tensor components of electronic and ionic gases, $\nu_{en}, \nu_{e+}, \nu_{+n}$ are the frequencies of electron-neutral, electron-ion, and ion-neutral collisions. Finally, $\mathbf{B}$ is the inductivity of magnetic field.

In view of the fact that $m_e \ll m_+$, and it follows that $\rho_e(\mathbf{u}_e \cdot \nabla)\mathbf{u}_e \ll \rho_+(\mathbf{u}_+ \cdot \nabla)\mathbf{u}_+$. In this case, it is possible to simplify Eq. (4) as follows:

$$-\nabla p_e - en_e\left(\mathbf{E} + \frac{1}{c}[\mathbf{u}_e\mathbf{B}]\right) - m_e\nu_{en}n_e(\mathbf{u}_e - \mathbf{u}_n) - m_e\nu_{e+}n_e(\mathbf{u}_e - \mathbf{u}_+) = 0. \tag{6}$$

Again, for $\mathbf{u}_e \gg \mathbf{u}_n, \mathbf{u}_+$ and $p_e = n_e kT_e[K]$, Eq. (4) can be further reduced,

$$kT_e\nabla n_e + en_e\mathbf{E} + \frac{en_e}{c}[\mathbf{u}_e\mathbf{B}] + (m_e\nu_e)n_e\mathbf{u}_e = 0. \tag{7}$$

Finally, it becomes

$$n_e\mathbf{u}_e = -D_e\nabla n_e - \mu_e n_e\mathbf{E} - \frac{\mu_e n_e}{c}[\mathbf{u}_e\mathbf{B}], \tag{8}$$

where $\mu_e = e/m_e\nu_e$ is the electron mobility, $D_e = ((kT_e[K])/e)\mu_e$ is the electron diffusion coefficient, and the averaged electron collision frequency is approximated by $\nu_e = \nu_{en} + \nu_{e+}$.

For the condition, the electron velocity has two components $\mathbf{u}_e = \{u_{e,x}; u_{e,y}\}$ and supposing that the magnetic field has only z component B_z (see Fig. 1), the charged particles flux densities become:

$$\Gamma_{e,x} = n_e u_{e,x} = \frac{1}{1+b_e^2}\left(-D_e\frac{\partial n_e}{\partial x} - \mu_e n_e E_x\right) - \frac{b_e}{1+b_e^2}\left(-D_e\frac{\partial n_e}{\partial y} - \mu_e n_e E_y\right), \tag{9}$$

$$\Gamma_{e,y} = n_e u_{e,y} = \frac{1}{1+b_e^2}\left(-D_e\frac{\partial n_e}{\partial y} - \mu_e n_e E_y\right) + \frac{b_e}{1+b_e^2}\left(-D_e\frac{\partial n_e}{\partial x} - \mu_e n_e E_x\right), \tag{10}$$

where $b_e = (\mu_e/c)B_z$; E_x, E_y are the components of the electric field intensity along the x and y coordinates, respectively.

Similarly, the momentum conservation of the ionic species also attains the following form

$$-\nabla p_+ + en_+\left(\mathbf{E} + \frac{1}{c}[\mathbf{u}_+\mathbf{B}]\right) - m_+\nu_{+e}n_+(\mathbf{u}_+ - \mathbf{u}_e) - m_+\nu_{+n}n_+(\mathbf{u}_+ - \mathbf{u}_n) = 0. \tag{11}$$

Assume that $m_+\nu_{+e}n_+(\mathbf{u}_+ - \mathbf{u}_e) = -m_e\nu_{e+}n_e(\mathbf{u}_e - \mathbf{u}_+)$, $\mathbf{u}_n = 0$, and $m_e\nu_e \ll m_+\nu_{+n}$, it is obtained

$$n_+\mathbf{u}_+ = -D_+\nabla n_+ + \mu_+ n_+\mathbf{E} + \frac{\mu_+ n_+}{c}[\mathbf{u}_+\mathbf{B}], \tag{12}$$

where $\mu_+ = e/(m_+\nu_{+n})$ is the ions mobility, $D_+ = ((kT_+[K])/e)\mu_+$ is the ions diffusion coefficient.

For the present two-dimensional analysis, the ions velocity has only two components $\mathbf{u}_+ = \{u_{+,x}; u_{+,y}\}$, and the magnetic field has only z-component B_z, we can write:

$$\Gamma_{+,x} = n_+ u_{+,x} = \frac{1}{1+b_+^2}\left(-D_+\frac{\partial n_+}{\partial x} + \mu_+ n_+ E_x\right) - \frac{b_+}{1+b_+^2}\left(-D_+\frac{\partial n_+}{\partial y} + \mu_+ n_+ E_y\right), \tag{13}$$

$$\Gamma_{+,y} = n_+ u_{+,y} = \frac{1}{1+b_+^2}\left(-D_+\frac{\partial n_+}{\partial y} + \mu_+ n_+ E_y\right) + \frac{b_+}{1+b_+^2}\left(D_+\frac{\partial n_+}{\partial x} - \mu_+ n_+ E_x\right) \tag{14}$$

where $b_+ = (\mu_+/c)B_z$. The effective electric field for the charged particles has a total of four components:

$$E_{e,x} = \frac{b_e E_y - E_x}{1+b_e^2}, \quad E_{e,y} = -\frac{b_e E_x + E_y}{1+b_e^2}, \tag{15}$$

$$E_{+,x} = \frac{E_x + b_+ E_y}{1 + b_+^2}, \quad E_{+,y} = \frac{E_y - b_+ E_x}{1 + b_+^2}. \tag{16}$$

Now continuity equations (1) and (2) can be generalized with using of the effective electric field components to appear as:

$$\frac{\partial n_e}{\partial t} + \frac{\partial}{\partial x}\left(\mu_e n_e E_{e,x} - \frac{D_e}{1 + b_e^2}\frac{\partial n_e}{\partial x}\right) + \frac{\partial}{\partial y}\left(\mu_e n_e E_{e,y} - \frac{D_e}{1 + b_e^2}\frac{\partial n_e}{\partial y}\right) = \alpha(E,p)|\Gamma_e| - \beta n_e n_+, \tag{17}$$

$$\frac{\partial n_+}{\partial t} + \frac{\partial}{\partial x}\left(\mu_+ n_+ E_{+,x} - \frac{D_+}{1 + b_+^2}\frac{\partial n_+}{\partial x}\right) + \frac{\partial}{\partial y}\left(\mu_+ n_+ E_{+,y} - \frac{D_+}{1 + b_+^2}\frac{\partial n_+}{\partial y}\right) = \alpha(E,p)|\Gamma_e| - \beta n_e n_+. \tag{18}$$

It should be noted that the introduced coefficients b_e, b_+ are the Hall parameters for electrons and ions, which are associated with a physically meaningful magnetic field:

$$b_e = \frac{\mu_e B_z}{c} = \frac{\omega_e}{\nu_e}, \quad b_+ = \frac{\mu_+ B_z}{c} = \frac{\omega_+}{\nu_+ \mathrm{n}}, \tag{19}$$

where $\omega_e = eB_z/m_e c$ is the Larmor frequency of electrons, $\omega_+ = eB_z/m_+ c$ is the Larmor frequency of ions.

It is well known by the work of Raizer [7] and Mitchner and Kruger [8] that Eqs. (1) and (2) are inadequate in describing the sheath regions of a space charge at the immediate vicinity to electrodes (cathode and anode). Therefore, many attempts were made to modify the diffusion-drift theory [4] or to use different numerical simulation models, including Monte Carlo simulation [12] for describing the sheath regions of the space charge. It was shown that improved theories can predict some new details of the glow discharge structure, but at the same time, the diffusion drift theory is still able to predict all general features of the glow discharge with sufficient accuracy for applied physics and different engineering applications. Therefore, the diffusion-drift model is adopted for the present analysis.

The fact mentioned above about the approximate character of the diffusion-drift theory in the immediate vicinity to the cathodes has the following consequence: the basic issue of inaccuracy arises from the inadequate boundary conditions implementation instead of the diffusion-drift theory. Therefore, we will analyze two modifications of the diffusion-drift theory. Raizer and Surzhikov [13] have studied the first approach in which the modification is based on the fact that the particles diffusion in the y-direction is negligible in comparison with the component in the x-direction. The second approach has also been investigated by Raizer and Surzhikov [14]. They took into account the diffusion in all directions, but used approximate boundary conditions for charged particle fluxes on electrodes.

To formulate these models, the typical behavior of the glow discharge is analyzed in the vicinity of electrodes. Fig. 2(a) and (b) depict a typical distribution of electron and ion concentrations, electrical field in glow discharge for nitrogen at a pressure of 5torr, with an electromotive force (Emf) of power supply of 3 kV, and an electrical resistance in the external circuit R_0 of 300 kΩ. These calculations are in good accordance with known experimental data on glow discharge [14], therefore these data will be used for evaluating all general parameters of a glow discharge: the volume concentration of ions in the cathode layer ($y < d_n$; d_n is the width of the cathode layer; $d_n \sim 0.1$ cm) is $(n_+)_{cl} \cong 3 \times 10^{10}$ cm^{-3}; the volume concentration of ions and electrons in the positive column ($0.1 \leqslant y \leqslant 1.9$ cm) is $(n_+)_{pc} = (n_e)_{pc} \cong 5 \times 10^9$ cm^{-3}; the maximal electric field intensity in the cathode layer is $(E)_{cl} = 4500$ V/cm; the electric field intensity in the positive column is $(E)_{pc} = 100$ V/cm; and the maximal electric field intensity in the anode layer $d_a \approx 0.1$ cm $1.9 \leqslant y \leqslant 2.0$ cm) is $(E)_{al} = 270$ V/cm.

Let the temperatures of electrons and ions be equal to $T_e = 1$ eV ($T_e = 11,610$ K), and $T_+ = 0.0258$ eV ($T_+ = 300$ K). In earlier numerical studies of a normal glow discharge structure at electronic temperature

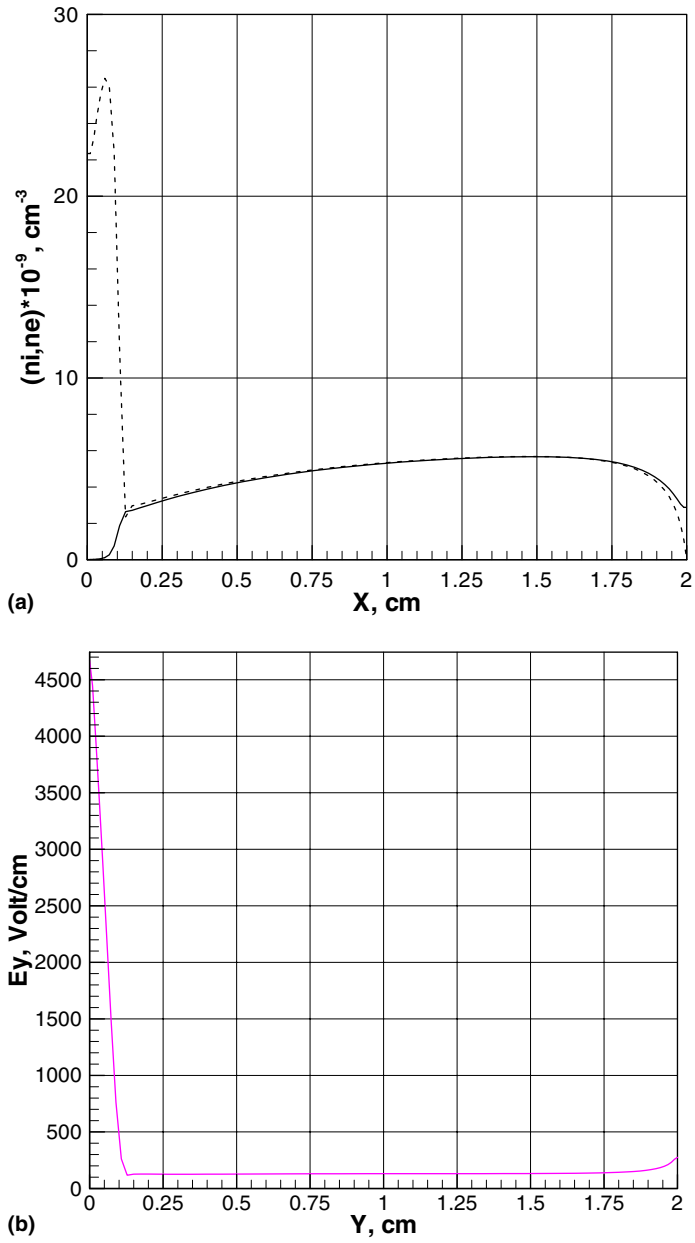

Fig. 2. (a) Distribution of electron (solid line) and ion (dashed line) concentrations in the column of glow discharge in N^2 at $p = 5$ torr and $E = 3$ kV. (b) Distribution of electric field intensity E_y in the column of glow discharge in N_2 at $p = 5$ torr and 3 kV.

up to 5 eV, all results showed that one could still use $T_e = 1$ eV as a reasonable approximation [13]. Under these conditions, electron and ion mobilities for glow discharge in N_2 can be approximated as follows [7]:

$$\mu_e = \frac{4.4 \times 10^5}{p} \frac{\text{cm}^2}{\text{s V}} \quad \text{and} \quad \mu_+ = \frac{1.45 \times 10^3}{p} \frac{\text{cm}^2}{\text{s V}}, \tag{20}$$

where p is the gas pressure in torr.

Using Einstein's formulas, one can get the estimation of electron and ion diffusion coefficients [6]

$$D_e = \mu_e T_e \ \frac{\mathrm{cm}^2}{s}, \quad D_+ = \mu_+ T_+ \ \frac{\mathrm{cm}^2}{s}. \tag{21}$$

For the present case ($p = 5$ torr), $\mu_e = 8.8 \times 10^4$ cm^2/s V, $\mu_+ = 290$ cm^2/s V, and $D_e = 8.8 \times 10^4$ cm^2/s, $D_+ = 7.48$ cm^2/s.

From these data, the diffusion and drift fluxes are calculated for electrons and ions in the y-direction

$$\Gamma_{e,y} = -D_e \frac{\partial n_e}{\partial y} - n_e \mu_e E_y = \Gamma_{e,y,\mathrm{dif}} + \Gamma_{e,y,\mathrm{dr}}, \quad \Gamma_{+,y} = -D_+ \frac{\partial n_+}{\partial y} + n_+ \mu_+ E_y = \Gamma_{+,y,\mathrm{dif}} + \Gamma_{+,y,\mathrm{dr}}, \tag{22}$$

where $E_y = -\partial\varphi/\partial y$, $\Gamma_{e,y,\mathrm{dif}}$, $\Gamma_{+,y,\mathrm{dif}}$ are the diffusion fluxes of electrons and ions in the y-direction, $\Gamma_{e,y,\mathrm{dr}}$, $\Gamma_{+,y,\mathrm{dr}}$ are the drift fluxes of electrons and ions in the y-direction, respectively.

These values in cathode and anode layers are used to determine the local electron and ion flux density.

In the cathode layer:

$$\left|\Gamma_{e,y,\mathrm{dif}}\right|_{\mathrm{cl}} \sim D_e \frac{(n_e)_{\mathrm{pc}}}{d_n} = 4.4 \times 10^{15}, \quad \left|\Gamma_{e,y,\mathrm{dr}}\right|_{\mathrm{cl}} \sim 0.1 (n_e)_{\mathrm{pc}} \mu_e E_{\mathrm{cl}} = 1.98 \times 10^{17} \ \frac{1}{\mathrm{cm}^2\,\mathrm{s}},$$
$$\left|\Gamma_{+,y,\mathrm{dif}}\right|_{\mathrm{cl}} \sim D_+ \frac{(n_+)_{\mathrm{cl}}}{d_n} = 2.24 \times 10^{12}, \quad \left|\Gamma_{+,y,\mathrm{dr}}\right|_{\mathrm{cl}} \sim (n_+)_{\mathrm{cl}} \mu_+ E_{\mathrm{cl}} = 3.9 \times 10^{16} \ \frac{1}{\mathrm{cm}^2\,\mathrm{s}},$$

where the factor 0.1 represents an average value of electronic concentration in cathode layer.

In the anode layer:

$$\left|\Gamma_{e,y,\mathrm{dif}}\right|_{\mathrm{al}} \sim D_e \frac{(n_e)_{\mathrm{pc}}}{d_a} = 4.4 \times 10^{15}, \quad \left|\Gamma_{e,y,\mathrm{dr}}\right|_{\mathrm{al}} \sim (n_e)_{\mathrm{pc}} \mu_e E_{\mathrm{al}} = 1.32 \times 10^{17} \ \frac{1}{\mathrm{cm}^2\,\mathrm{s}},$$
$$\left|\Gamma_{+,y,\mathrm{dif}}\right|_{\mathrm{al}} \sim D_+ \frac{(n_+)_{\mathrm{pc}}}{d_a} = 3.74 \times 10^{11}, \quad \left|\Gamma_{+,y,\mathrm{dr}}\right|_{\mathrm{al}} \sim (n_+)_{\mathrm{pc}} \mu_+ E_{\mathrm{al}} = 4.35 \times 10^{14} \ \frac{1}{\mathrm{cm}^2\,\mathrm{s}}.$$

It is clear from the order of magnitude analysis that

$$\begin{aligned} &\left|\Gamma_{e,y,\mathrm{dr}}\right|_{\mathrm{cl}} \gg \left|\Gamma_{e,y,\mathrm{dif}}\right|_{\mathrm{cl}}, \quad \left|\Gamma_{+,y,\mathrm{dr}}\right|_{\mathrm{cl}} \gg \left|\Gamma_{+,y,\mathrm{dif}}\right|_{\mathrm{cl}}, \\ &\left|\Gamma_{e,y,\mathrm{dr}}\right|_{\mathrm{al}} \gg \left|\Gamma_{e,y,\mathrm{dif}}\right|_{\mathrm{al}}, \quad \left|\Gamma_{+,y,\mathrm{dr}}\right|_{\mathrm{al}} \gg \left|\Gamma_{+,y,\mathrm{dif}}\right|_{\mathrm{al}}. \end{aligned} \tag{23}$$

It should be noted that in the immediate vicinity of the cathode (where $n_e \ll n_+$), electronic diffusion and drift fluxes might be commensurable. Thus, in the sheath region the diffusion-drift theory may no longer hold. The diffusion of electrons is very significant in the Faraday region of the glow discharge, for the case considered, this region is at a distance around 0.1 cm from the cathode. Therefore, the model of ionization with $\alpha = \alpha(E)$ cannot be adequately predicted by the behavior of particle distributions in this region, because the non-local effects of ionization can be very significant [6,7]. Nevertheless, this very week region of a glow discharge will be omitted from the present consideration.

Some words should be added also concerning the chemical composition of a direct glow discharge under consideration. It is well known that glow discharge plasma of molecular nitrogen contains not only such obvious components as N_2, N_2^+ and electrons (e^-), but also N_4^+ and other vibrationally and electronically excited molecules and atoms [3–7]. But using semi-empirical diffusion-drift model of the glow discharge allows us to describe the peculiarities of electrodynamics of different species and their populations on excited energetic levels (including electron distributions on velocities) by introduction of empirical coefficients. They are: the first Townsend ionization coefficient and recombination coefficient β (see later).

If such model is developed for description of direct glow discharges in such electronegative gases as air, then charge kinetics of negative ions O_2^-, O^-, O_3^-, O_4^-, NO^-, NO_2^-, NO_3^- should be taken into consideration. This problem is much more difficult. Nevertheless, it is still possible to formulate in the frame of a semi-empirical diffusion-drift model by additional equations for negative charged particles and some empirical coefficients for attachment and detachment of electrons to atoms and molecules. It is also possible in the framework of the two-fluid model by introduction of the effective coefficient of recombination. In fact, Raizer showed that one can use $\beta_{\text{effective}} \approx 40\beta$ but this is a very rough approximation and needs further study.

3. Approximate boundary conditions and two models of DCGD

The vast difference of diffusion components in sheath regions allows Raizer and Surzhikov [13,14] to postulate a numerical model of glow discharge by neglecting the diffusion in the y-direction. This assumption essentially simplified the formulation of boundary conditions, because in this case the order of Eqs. (1) and (2) was reduced by one.

Now the electron and ion fluxes can be written in the following form;

$$\Gamma_e = -D_e \operatorname{grad}_x n_e - n_e \mu_e \mathbf{E}, \tag{24}$$

$$\Gamma_+ = -D_+ \operatorname{grad}_x n_+ + n_+ \mu_+ \mathbf{E}, \tag{25}$$

where $\operatorname{grad}_x = \mathbf{e}_x(\partial/\partial x) + \mathbf{e}_y \cdot 0 = \mathbf{e}_x(\partial/\partial x)$, and $\mathbf{e}_x$, $\mathbf{e}_y$ are the unit vectors of x and y coordinates, respectively.

The boundary conditions for electronic and ionic fluxes on electrodes are analyzed as follows. The electronic and ionic fluxes to the cathode (without diffusion in the y-direction) are determined by (24) and (25). Since the general mechanism of electronic emission from the cathode is the secondary electronic emission [3–6], it yields

$$(\Gamma_e)_{y=0} = -\gamma(\Gamma_+)_{y=0}, \tag{26}$$

where γ is the coefficient of the secondary electronic emission. This coefficient depends on a material of a cathode and intensity of electronic field. Von Engel and Steenbeck [3], Brown [5] and Raizer [7] have extensively analyzed the influence of γ on the structure of gas discharge. A range of γ values from 10^{-1} to 10^{-2} were recommended for numerical study of a glow discharge structure in nitrogen [13]. As it is noted that using an overestimated value of the secondary emission coefficient (for example, $\gamma = 0.3$) led to an improvement of computational stability [13]. Therefore, some present calculations were performed with this value of γ.

Eqs. (24)–(26) give

$$(n_e)_{y=0} = \gamma(n_+)_{y=0}\frac{\mu_+}{\mu_e}. \tag{27}$$

As far as the boundary conditions for the anode are concerned, it is assumed that the anode reflects all ions and the ion flux in the y-direction is much greater than in the x-direction:

$$|\Gamma_+|_{y,\mathrm{dr}} \gg |\Gamma_+|_{x,\mathrm{dr}} + |\Gamma_+|_{x,\mathrm{dif}}.$$

Then, one can get at $y = H$, $(\Gamma_+)_y = 0$, and $n_+ = 0$.

It should be stressed that from the physical viewpoint, any additional boundary conditions for solving the system of equations (1)–(3) are unnecessary.

Immediately adjacent to the cathode and anode surface, the approximate boundary conditions of the vanishing Neumann type are appropriate to describe the negligible diffusion component. In fact, this type

of numerical boundary condition is widely used in electromagnetic computations near media interfaces, where the transverse electromagnetic field gradient is dominated over the normal component [16]. For the present purposes, the continuity equation for the space charge is further developed to implement the numerical boundary condition:

$$\frac{\partial \rho}{\partial t} + \operatorname{div}(\Gamma_+ - \Gamma_e) = 0, \tag{28}$$

where $\rho = n_+ - n_e$.

In the vicinity to cathode $n_e \ll n_+$, from Eq. (26), one can get

$$\frac{\partial n_+}{\partial t} = (1 \pm \gamma)\mu_+ \frac{\partial}{\partial y}\left(n_+ \frac{\partial \varphi}{\partial y}\right) - D_{c,\mathrm{eff}} \frac{\partial^2 n_+}{\partial x^2}, \tag{29}$$

where

$$D_{c,\mathrm{eff}} = D_e \gamma \frac{\mu_+}{\mu_e} - D_+. \tag{30}$$

All numerical experiments show that the results by the following boundary condition $(\partial n_+/\partial y)_{y=0} = 0$ are very closely approximated to the prediction by Eq. (29). In addition, this approximate boundary condition is computationally stable.

Similarly, one can apply the approximate boundary condition for electrons on the anode:

$$\frac{\partial n_e}{\partial t} = -\mu_e \frac{\partial}{\partial y}\left(n_e \frac{\partial \varphi}{\partial y}\right) + D_e \frac{\partial^2 n_e}{\partial x^2}. \tag{31}$$

The present model without diffusion in y-direction, the governing equations of glow discharge (1)–(3) are simplified, where Γ_e and Γ_+ now are determined by Eqs. (24) and (25).

Boundary conditions in this case are; at $y = 0 : n_e = \gamma n_+(\mu_+/\mu_e), \varphi = 0$. The additional approximate boundary condition is:

$$\frac{\partial n_+}{\partial t} = (1 + \gamma)\mu_+ \frac{\partial}{\partial y}\left(n_+ \frac{\partial \varphi}{\partial y}\right) - D_{c,\mathrm{eff}} \frac{\partial^2 n_+}{\partial x^2}. \tag{32}$$

At $y = H$: $n_i = 0,\ \varphi = V$, the approximate boundary condition becomes:

$$\frac{\partial n_e}{\partial t} = -\mu_e \frac{\partial}{\partial y}\left(n_e \frac{\partial \varphi}{\partial y}\right) - D_e \frac{\partial^2 n_e}{\partial x^2}. \tag{33}$$

$$\text{At } y = 0, L: \quad \frac{\partial n_e}{\partial y} = \frac{\partial n_+}{\partial y} = \frac{\partial \varphi}{\partial y} = 0. \tag{34}$$

Here V is the voltage drops across the gas discharge gap, H, L are height and transversal scale of the gas discharge channel, respectively.

The second approach to expand the applicable envelope of the diffusion-drift model into sheath region is outlined as follows. In this approach, the neglected diffusion of charged particles in the y-direction is modeled by using well-known classic results [7]. To simplify our analysis, let us consider one-dimensional glow discharge (in the y-direction):

$$\frac{\partial n_e}{\partial t} + \frac{\partial \Gamma_e}{\partial y} = \alpha(E, p)\Gamma_e - \beta n_e n_+, \tag{35}$$

$$\frac{\partial n_+}{\partial t}+\frac{\partial \Gamma_\mathrm{i}}{\partial y}=\alpha(E,p)\Gamma_\mathrm{e}-\beta n_\mathrm{e}n_+, \tag{36}$$

Now the flux densities reduce to $\Gamma_\mathrm{e}=-n_\mathrm{e}\mu_\mathrm{e}E_y-D_\mathrm{e}(\partial n_\mathrm{e}/\partial y)$, $\Gamma_+=n_+\mu_+E_y-D_+(\partial n_+/\partial y)$ and $(\partial E_y/\partial y)=4\pi e(n_+-n_\mathrm{e})$.

The formulas for the electronic flux are based on the Lorenz approximation for the electronic distribution function on velocities $\mathbf{V}_\mathrm{e}$ [7]:

$$f(\mathbf{V}_\mathrm{e})=f_0(V)+f_1(V)\cos\theta, \tag{37}$$

where θ is the angle between $\mathbf{V}_\mathrm{e}$ and y, f_0, f_1 are the coefficients of expansion of the distribution function, $V=|\mathbf{V}_\mathrm{e}|$.

Introduce the half-spherical fluxes as:

$$\begin{aligned}\Gamma_\mathrm{e}^{\pm}&=2\pi\int\int V\cos\theta(f_0+f_1\cos\theta)V^2\,\mathrm{d}V\sin\theta\,\mathrm{d}\theta=\frac{n_\mathrm{e}\bar{V}_\mathrm{e}}{4}\pm\frac{\Gamma_\mathrm{e}}{2}\\&=\frac{n_\mathrm{e}\bar{V}_\mathrm{e}}{4}\pm\frac{1}{2}\left(-\mu_\mathrm{e}n_\mathrm{e}E_y-D_\mathrm{e}\frac{\partial n_\mathrm{e}}{\partial y}\right),\end{aligned} \tag{38}$$

where $\bar{V}_\mathrm{e}$ is the averaged thermal velocity of electrons, $\bar{V}_\mathrm{e}=\sqrt{8kT_\mathrm{e}/\pi m_\mathrm{e}}\approx 6.21\times 10^5\sqrt{T_\mathrm{e}\ [\mathrm{K}]}=6.71\times 10^7\sqrt{T_\mathrm{e}\ [\mathrm{eV}]}$ cm/s, $D_\mathrm{e}=\mu_\mathrm{e}T_\mathrm{e}=1\bar{V}_\mathrm{e}/3$, and l is the electronic free path. If the cathode only reflects and emits electrons without absorption, then $\Gamma_\mathrm{e}^+=\Gamma_\mathrm{e}^--\gamma\Gamma_+$, then as before $\Gamma_\mathrm{e}=\Gamma_\mathrm{e}^+-\Gamma_\mathrm{e}^-=-\gamma\Gamma_+$. Near the anode we will use the following physical boundary condition, $\Gamma_\mathrm{e}^-=0$. In other words, the anode does not reflect electrons. Then it yields,

$$\frac{n_\mathrm{e}\bar{V}_\mathrm{e}}{4}+\frac{1}{2}\mu_\mathrm{e}n_\mathrm{e}E+\frac{1}{2}D_\mathrm{e}\frac{\partial n_\mathrm{e}}{\partial y}=0\quad\text{or}\quad\frac{\partial n_\mathrm{e}}{\partial y}=\frac{1}{D_\mathrm{e}}\left(\mu_\mathrm{e}n_\mathrm{e}\frac{\partial\varphi}{\partial y}-n_\mathrm{e}\frac{\bar{V}_\mathrm{e}}{2}\right). \tag{39}$$

As for ions: $|\Gamma_{+,\mathrm{dr}}|\gg|\Gamma_{+,\mathrm{dif}}|$, the physical condition of $\Gamma_+^+=0$ leads to $n_\mathrm{i}=0$.

Now return to the other possible approximate boundary condition [14]. The model equation with diffusion in the y-direction is formulated in the form (1)–(3), where

$$\Gamma_{\mathrm{e},x}=n_\mathrm{e}\mu_\mathrm{e}\frac{\partial\varphi}{\partial x}-D_\mathrm{e}\frac{\partial n_\mathrm{e}}{\partial x},\quad\Gamma_{\mathrm{e},y}=n_\mathrm{e}\mu_\mathrm{e}\frac{\partial\varphi}{\partial y}-D_\mathrm{e}\frac{\partial n_\mathrm{e}}{\partial y},\quad\Gamma_{+,x}=-n_+\mu_+\frac{\partial\varphi}{\partial x}-D_+\frac{\partial n_+}{\partial x}\quad\text{and}$$
$$\Gamma_{+,y}=-n_+\mu_+\frac{\partial\varphi}{\partial y}-D_+\frac{\partial n_+}{\partial y}$$

Finally, boundary conditions for the system of equations become:

$$\text{At } y=0:\quad n_\mathrm{e}=\gamma n_+\frac{\mu_+}{\mu_\mathrm{e}},\quad\varphi=0, \tag{40}$$

$$\frac{\partial n_+}{\partial t}=(1+\gamma)\mu_+\frac{\partial}{\partial y}\left(n_+\frac{\partial\varphi}{\partial y}\right)-D_{\mathrm{c,eff}}\frac{\partial^2 n_+}{\partial x^2}, \tag{41}$$

$$\text{At } y=H:\quad\frac{\partial n_\mathrm{e}}{\partial y}=\frac{1}{D_\mathrm{e}}\left(\mu_\mathrm{e}n_\mathrm{e}\frac{\partial\varphi}{\partial y}-n_\mathrm{e}\frac{\bar{V}_\mathrm{e}}{2}\right), \tag{42}$$

$$n_\mathrm{i}=0,\quad\varphi=V, \tag{43}$$

$$\text{At } y = 0, \quad L : \frac{\partial n_e}{\partial y} = \frac{\partial n_+}{\partial y} = \frac{\partial \varphi}{\partial y} = 0. \tag{44}$$

In the present investigation, the constitutive relationship can be determined easily if the temperature of neutral species is assumed to be a constant. The transport and thermo-physics properties are therefore not dependent on the temperature. The recombination coefficient β and electron temperature are taken as constants $\beta = 2 \times 10^{-7}$ cm^3/s [7].

The ionization coefficient is determined by the Townsend formula [3–6]:

$$\alpha(E,p) = pA \exp\left[-\frac{B}{(|\mathbf{E}|/p)} \right] \text{ cm}^{-1}, \tag{45}$$

where the dimensional constants are given as $A = 12$ (cm torr)$^{-1}$ and $B = 342$ V/(cm torr).

These equations for boundary conditions are supplemented with the equation for the external circuit (see Fig. 1), which is written for a stationary current as $E = V + IR_0$, where V is the voltage on the electrodes, I is the total discharge current, E is the Emf of the power supply, and R_0 is the external resistance.

4. Governing equations for numerical solution

The continuity equations for charged particles and the Poisson equation for electric potential can be written in the following form

$$\frac{\partial u}{\partial \tau} + \frac{\partial au}{\partial \tilde{x}} + \frac{\partial bu}{\partial \tilde{y}} = \frac{\partial}{\partial \tilde{x}}\left(D \frac{\partial u}{\partial \tilde{x}} \right) + \frac{\partial}{\partial \tilde{y}}\left(D \frac{\partial u}{\partial \tilde{y}} \right) + f, \tag{46}$$

where the independent and dependent variables are normalized with respect to the relevant characteristic dimensions: $\tilde{x} = x/H,\ \tilde{y} = y/H,\ \tau = t/t_0,\ t_0 = H^2/\mu_{e,0}E;\ u = \{n_e, n_+, \varphi\}$.

This equation is used to obtain the steady asymptote to the Poisson equation, therefore the time t is actually adopted as an iterative parameter in the present approach.

Coefficients a, b, D and functions u, f are given by the following formulas:

(a) For electrons:

$$u = u_e = \frac{n_e}{N_0}, \quad a = \tilde{\mu}_e \frac{\partial \Phi}{\partial \tilde{x}}, \quad b = \tilde{\mu}_e \frac{\partial \Phi}{\partial \tilde{y}}, \quad D = \tilde{D}_e,$$

$$f = f_e = \alpha H \sqrt{\left(u_e \tilde{\mu}_e \frac{\partial \Phi}{\partial \tilde{x}} - \tilde{D}_e \frac{\partial u_e}{\partial \tilde{x}} \right)^2 + \left(u_e \tilde{\mu}_e \frac{\partial \Phi}{\partial \tilde{y}} - \tilde{D}_e \frac{\partial u_e}{\partial \tilde{y}} \right)^2} - \beta \frac{H^2 N_0}{\mu_{e,0} E} u_e u_+,$$

where $\tilde{\mu}_e = \mu_e/\mu_{e,0},\ \Phi = \varphi/E,\ \tilde{D}_e = D_e/\mu_{e,0}E,\ u_+ = n_+/N_0;\ \mu_{e,0}$ is the representative value of the electron mobility, for example, $\mu_{e,0} = \mu_e$ at $p = 5$ torr, and N_0 is the typical concentration of charged particles in positive column, in the present case, $N_0 = 10^9$ cm^{-3}.

(b) For ions:

$$u = u_+ = \frac{n_+}{N_0}, \quad a = -\tilde{\mu}_+ \frac{\partial \Phi}{\partial \tilde{x}}, \quad b = -\tilde{\mu}_+ \frac{\partial \Phi}{\partial \tilde{y}}, \quad D = \tilde{D}_+, \quad f = f_e,$$

where $\tilde{\mu}_+ = \mu_+/\mu_{e,0},\ \tilde{D}_+ = D_+/\mu_{e,0}E$.

(c) For the Poisson equation: $a = b = 0, \quad D = 1, \quad f = \varepsilon(u_+ - u_e)$, where $\varepsilon = 4\pi e(H^2 N_0/E),\ 4\pi e = 1.86 \times 10^{-6}$ V.

In summary, the specific initial values and the boundary conditions can be given as

(1) For electrons without diffusion in the y-direction:

$$\tilde{y}=0: \quad u_{\mathrm{e}}=\gamma u_{+}\frac{\tilde{\mu}_{+}}{\tilde{\mu}_{\mathrm{e}}},$$
$$\tilde{y}=1: \quad \frac{\partial u_{\mathrm{e}}}{\partial\tau}=-\tilde{\mu}_{\mathrm{e}}\frac{\partial}{\partial\tilde{y}}\left(u_{\mathrm{e}}\frac{\partial\Phi}{\partial\tilde{y}}\right)-\tilde{D}_{\mathrm{e}}\frac{\partial^{2}u_{\mathrm{e}}}{\partial\tilde{x}^{2}},$$
$$\tilde{x}=0,\frac{L}{H}: \quad \frac{\partial u_{\mathrm{e}}}{\partial\tilde{x}}=0.$$

(2) For ions without diffusion in the y-direction

$$\tilde{y}=0: \quad \frac{\partial u_{+}}{\partial\tau}=(1+\gamma)\tilde{\mu}_{+}\frac{\partial}{\partial\tilde{y}}\left(u_{+}\frac{\partial\Phi}{\partial\tilde{y}}\right)-\tilde{D}_{\mathrm{c,eff}}\frac{\partial^{2}u_{+}}{\partial\tilde{x}^{2}},$$

where $\tilde{D}_{\mathrm{c,eff}}=(D_{\mathrm{c,eff}})/(\mu_{\mathrm{e},0}E)$,

$$\tilde{y}=1: \quad u_{+}=0,$$
$$\tilde{x}=0,\frac{L}{H}: \quad \frac{\partial u_{+}}{\partial\tilde{x}}=0.$$

(3) For electrons with diffusion in the y-direction

$$\tilde{y}=0: \quad u_{\mathrm{e}}=\gamma u_{+}\mu_{+}\frac{\tilde{\mu}_{+}}{\tilde{\mu}_{\mathrm{e}}},$$
$$\tilde{y}=1: \quad \tilde{D}_{\mathrm{e}}\frac{\partial u_{\mathrm{e}}}{\partial\tilde{y}}=\tilde{\mu}_{\mathrm{e}}u_{\mathrm{e}}\frac{\partial\Phi}{\partial\tilde{y}}-u_{\mathrm{e}}\frac{\tilde{V}_{\mathrm{e}}H}{2\mu_{\mathrm{e},0}E},$$
$$\tilde{x}=0,\frac{L}{H}: \quad \frac{\partial u_{\mathrm{e}}}{\partial\tilde{x}}=0.$$

(4) For ions with diffusion in the y-direction

$$\tilde{y}=0: \quad \frac{\partial u_{+}}{\partial\tau}=(1+\gamma)\tilde{\mu}_{+}\frac{\partial}{\partial\tilde{y}}\left(u_{+}\frac{\partial\Phi}{\partial\tilde{y}}\right)-\tilde{D}_{\mathrm{c,eff}}^{2}\frac{\partial^{2}u_{+}}{\partial\tilde{x}^{2}},$$
$$\tilde{y}=1: \quad u_{+}=0,$$
$$\tilde{x}=0,\frac{L}{H}: \quad \frac{\partial u_{+}}{\partial\tilde{x}}=0.$$

(5) For electric potential:

$$\tilde{y}=0: \quad \Phi=0,$$
$$\tilde{y}=1: \quad \Phi=E,$$
$$\tilde{x}=0,\frac{L}{H}: \quad \frac{\partial\Phi}{\partial\tilde{x}}=0.$$

It should be stressed that all boundary conditions, including components of effective electric field with external magnetic field were studied as computing experiments. Computations were guided by much more simplified boundary conditions to yield the final solution for integral parameters and species distributions

in computational domain away from the immediate vicinity of electrodes. In addition, the following boundary conditions are computationally stable, they are:

(I) For electrons

$$\tilde{y} = 0: \quad u_e = \gamma u_+ \frac{\tilde{\mu}_+}{\tilde{\mu}_e}, \tag{47}$$

$$\tilde{y} = 1: \quad \frac{\partial u_e}{\partial \tilde{y}} = 0, \tag{48}$$

$$\tilde{x} = 0, \frac{L}{H}: \quad \frac{\partial u_e}{\partial \tilde{x}} = 0. \tag{49}$$

(II) For ions without diffusion in the y-direction

$$\tilde{y} = 0: \quad \frac{\partial u_+}{\partial \tilde{y}} = 0, \tag{50}$$

$$\tilde{y} = 1: \quad u_+ = 0, \tag{51}$$

$$\tilde{x} = 0, \frac{L}{H}: \quad \frac{\partial u_+}{\partial \tilde{x}} = 0. \tag{52}$$

The numerical procedure used in this study is based on the two-stage calculations. A steady-state solution for glow discharge without magnetic field at given initial conditions was firstly obtained. Then, this numerical solution was used as initial condition for second-stage calculations with magnetic field. This procedure is necessary, because approximate initial conditions were used for the first-stage calculations. These initial conditions were based on the one-dimensional theory of the normal glow discharge, developed by Engel and Steenbeck [3]. Although the theoretical results provided reasonable values for the initial discharge plasma parameters, they do not satisfy rigorously the required two-dimensional boundary conditions:

$$\frac{j_n}{p^2} = 5.92 \times 10^{-11} \frac{AB^2 \mu_+ p(1+\gamma)}{\ln(1+\frac{1}{\gamma})} \ \mu\mathrm{A}/(\mathrm{cm}^2\,\mathrm{torr}^2), \tag{53}$$

$$d_n p = 3.78 A^{-1} \ln\left(1 + \frac{1}{\gamma}\right) \ \mathrm{cm\,torr}, \tag{54}$$

$$V_n = 3BA^{-1} \ln\left(1 + \frac{1}{\gamma}\right) \ \mathrm{V}, \tag{55}$$

where j_n is the normal current density, d_n is the thickness of a cathode layer, V_n is the voltage drop on the cathode layer, p is the pressure in torr; A, B are the approximation coefficients in the Townsend formula [3–7].

The volume concentration of ions in the cathode layer can be estimated. For the present purpose, a simplified formula for current density $j_n = e(n_e \mu_e E_y + n_+ \mu_+ E_y) = e(1+\gamma) n_+ \mu_+ E_y$ is used, and $E_y \approx V_n/d_n$. Similarly, one can obtain

$$n_{+,0} \approx \frac{j_n d_n}{e(1+\gamma)V_n \mu_+}, \quad n_{e,0} \approx n_{+,0}\gamma \frac{\mu_+}{\mu_e}.$$

In the positive column $(n_+)_{pc} = (n_e)_{pc} \approx 10^9$ cm^{-3}, therefore volume concentrations of ions and electrons in the cathode layer can be approximated as $n_+(x=0,y) = (n_+)_{pc} + (n_+)_0 \exp(-(y/d_n))$ and $n_e(x=0,y) = n_{e,0} + (n_e)_{pc}[1 - \exp(-y/(d_n))]$.

An estimation of the total current for a glow discharge in an axisymmetrical geometry gives $\dot{I} = j_n \pi L_c^2 = (E - 2V_n)/(R_0)$, where L_c is the radius of the current column, E, R_0 are the Emf of power supply and resistance in external electric circuit, respectively. The coefficient of '2' in the circuit equation yields a total voltage drop across the discharge gap. Again from this equation, an approximate dimension of the current column $L_c \approx \sqrt{(E - 2V_n)/(j_n \pi R_0)}$ is obtainable.

To predict parameters of glow discharge for a plane geometry, all integral parameters should be related to 1 cm of length in the z-direction. In this case, the above formula gives the estimated thickness of a current column in the plane geometry.

The two-dimensional distributions of charged particles for the initial conditions are calculated as follows:

$$n_e(x,y) = n_e(x=0,y) \exp\left[-\left(\frac{x}{L_c}\right)^3\right], \quad n_+(x,y) = n_+(x=0,y) \exp\left[-\left(\frac{x}{L_c}\right)^3\right].$$

5. Finite different scheme

The grid system of the present analysis is presented in Fig. 3. A five-point finite-difference scheme is adopted by integrating Eq. (47) over the shaded volume:

$$A_{i,j} u_{i-1,j}^{m+1} + B_{i,j} u_{i+1,j}^{m+1} + \bar{A}_{i,j} u_{i,j-1}^{m+1} + \bar{B}_{i,j} u_{i,j+1}^{m+1} - C_{i,j} u_{i,j}^{m+1} + F_{i,j}^{m+1/2} = 0. \tag{56}$$

The coefficients of the discretized pentadiagonal matrix system are:

$$\begin{aligned}
A_{i,j} &= a_L^+/\nabla x_i + D_{i-1/2,j}/\nabla x_i^- \nabla x_i, \quad B_{i,j} = -a_R^-/\nabla x_i + D_{i+1/2,j}/\nabla x_i^+ \nabla x_i, \\
\bar{A}_{i,j} &= b_L^+/\nabla y_j + D_{i,j-1/2}/\nabla y_j^- \nabla y_j, \quad \bar{B}_{i,j} = -b_R^-/\nabla x_i + D_{i,j+1/2}/\nabla y_j^+ \nabla y_j, \\
C_{i,j} &= 1/\tau + \left(a_R^+ - a_L^-\right)/\nabla x_i + \left(b_R^+ - b_L^-\right)/\nabla y_i + \left(D_{i+1/2,j}/\nabla x_i^+ + D_{i-1/2,j}/\nabla x_i^-\right)/\nabla x_i \\
&\quad + \left(D_{i,j+1/2}/\nabla y_j^+ + D_{i,j-1/2}/\nabla y_j^-\right)/\nabla y_j,
\end{aligned}$$

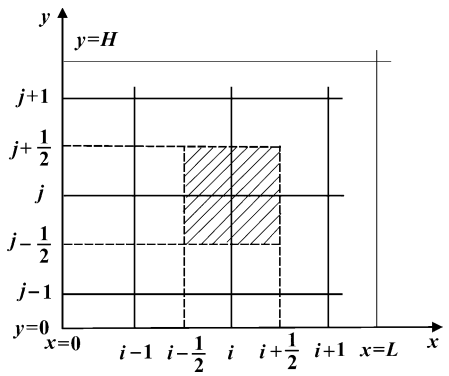

Fig. 3. Coordinates and grid structure.

and $F_{i,j} = ((u^m_{i,j})/\tau) + f^{m+1/2}_{i,j}$, where m is the index of the time increment, and

$$\nabla x_i = \left(\tilde{x}_{i+1} - \tilde{x}_{i-1}\right), \quad \nabla x^-_i = \left(\tilde{x}_i - \tilde{x}_{i-1}\right), \quad \nabla x^+_i = \left(\tilde{x}_{i+1} - \tilde{x}_i\right),$$
$$\nabla y_j = \left(\tilde{y}_{j+1} - \tilde{y}_{j-1}\right), \quad \nabla y^-_j = \left(\tilde{y}_j - \tilde{y}_{j-1}\right), \quad \nabla y^+_i = \left(\tilde{y}_{j+1} - \tilde{y}_j\right),$$
$$D_{i\pm1/2,j} = \tfrac{1}{2}\left(D_{i,j} + D_{i\pm1,j}\right), \quad D_{i,j\pm1/2} = \tfrac{1}{2}\left(D_{i,j} + D_{i,j\pm1}\right),$$
$$a_{\mathrm{R}} = \tfrac{1}{2}\left(a_{i,j} + a_{i+1,j}\right), \quad a_{\mathrm{L}} = \tfrac{1}{2}\left(a_{i,j} + a_{i-1,j}\right),$$
$$a^{\pm}_{\mathrm{R}} = \tfrac{1}{2}(a_{\mathrm{R}} \pm |a_{\mathrm{R}}|), \quad a^{\pm}_{\mathrm{L}} = \tfrac{1}{2}(a_{\mathrm{L}} \pm |a_{\mathrm{L}}|),$$
$$b_{\mathrm{R}} = \tfrac{1}{2}\left(b_{i,j} + b_{i,j+1}\right), \quad b_{\mathrm{L}} = \tfrac{1}{2}\left(b_{i,j} + b_{i,j-1}\right),$$
$$b^{\pm}_{\mathrm{R}} = \tfrac{1}{2}(b_{\mathrm{R}} \pm |b_{\mathrm{R}}|), \quad b^{\pm}_{\mathrm{L}} = \tfrac{1}{2}(b_{\mathrm{L}} \pm |b_{\mathrm{L}}|).$$

Boundary conditions are presented in the following formulas:

$$u_{i,1} = \alpha_i u_{i,2} + \beta_i, \quad i = 1, 2, \ldots, NI,$$
$$u_{i,NJ} = \bar{\alpha}_i u_{i,NJ-1} + \bar{\beta}_i, \quad i = 1, 2, \ldots, NI,$$
$$u_{1,j} = \gamma_j u_{2,j} + \delta_j, \quad j = 1, 2, \ldots, NJ,$$
$$u_{NI,j} = \bar{\gamma}_j u_{NI-1,j} + \bar{\delta}_j, \quad j = 1, 2, \ldots, NJ.$$

Formulations for coefficients $\alpha_i, \beta_i, \gamma_i, \delta_i, \bar{\alpha}_i, \bar{\beta}_i, \bar{\gamma}_i, \bar{\delta}_i$ in this finite-different representation of boundary conditions were derived from boundary conditions (40)–(44) for each dependent variables $u = \{n_{\mathrm{e}}, n_+, \varphi\}$.

Function $F^{m+1/2}_{i,j}$ contains non-linear components

$$f^{m+1/2}_{i,j} = \left[\alpha\left(E_{i,j}, p\right)|\Gamma_{\mathrm{e}}|_{\{i,j\}} - \beta n_{\mathrm{e}_{i,j}} n_{+_{i,j}}\right]^{m+1/2}.$$

Stability of the present numerical algorithm depends strongly on finite-different approximation of ionization rate $\alpha(E)|\Gamma_{\mathrm{e}}|$, because the function $\alpha(E)$ is an exponential function of E, which depends on the distribution of charged particles.

Module of electronic flux is approximated as follows:

$$|\Gamma_{\mathrm{e}}|_{i,j} = \sqrt{(\Gamma_{\mathrm{e},x})^2_{i,j} + \left(\Gamma_{\mathrm{e},y}\right)^2_{i,j}},$$

where

$$(\Gamma_{\mathrm{e},x})_{i,j} = u^{m+1/2}_{\mathrm{e},i-1,j}\tilde{\mu}_{\mathrm{e}}E^+_{x,i,j} - u^{m+1/2}_{\mathrm{e},i+1,j}\tilde{\mu}_{\mathrm{e}}E^-_{x,i,j} - \tilde{D}_{\mathrm{e},i,j}\frac{u^{m+1/2}_{\mathrm{e},i+1,j} - u^{m+1/2}_{\mathrm{e},i-1,j}}{\tilde{x}_{i+1} - \tilde{x}_{i-1}},$$
$$\left(\Gamma_{\mathrm{e},y}\right)_{i,j} = u^{m+1/2}_{\mathrm{e},i,j-1}\tilde{\mu}_{\mathrm{e}}E^+_{y,i,j} - u^{m+1/2}_{\mathrm{e},i,j+1}\tilde{\mu}_{\mathrm{e}}E^-_{y,i,j} + \tilde{D}_{\mathrm{e},i,j}\frac{u^{m+1/2}_{\mathrm{e},i,j+1} - u^{m+1/2}_{\mathrm{e},i,j-1}}{\tilde{y}_{j+1} - \tilde{y}_{j-1}},$$
$$E^{\pm}_{x,i,j} = \tfrac{1}{2}\left(E_{x,i,j} \pm \left|E_{x,i,j}\right|\right), \quad E^{\pm}_{y,i,j} = \tfrac{1}{2}\left(E_{y,i,j} \pm \left|E_{y,i,j}\right|\right),$$
$$E_{x,i,j} = -\frac{\Phi_{i+1,j} - \Phi_{i-1,j}}{\tilde{x}_{i+1} - \tilde{x}_{i-1}}, \quad E_{y,i,j} = -\frac{\Phi_{i,j+1} - \Phi_{i,j-1}}{\tilde{y}_{j+1} - \tilde{y}_{j-1}},$$
$$E_{i,j} = \sqrt{E^2_{x,i,j} + E^2_{y,i,j}}.$$

An iterative numerical procedure is used to facilitate the temporal evolution of solutions. Hence, the index $m + 1/2$ indicates the additional iterations on each time step. The iterative convergent criterion is set for the difference of consecutive solutions to be less than 10^{-5} in relative magnitude.

6. Numerical procedure and time scales

Finite different equation (56) is solved by an implicit finite-difference method. The fractional step iteration process was adopted on a stretched grid [17,18]

$$\{x_i,\ i = 1,2,\ldots,NI;\ x_1 = 0,\ x_{NI} = L;\ y_j,\ j = 1,2,\ldots,NJ;$$
$$y_j = 0,\ y_{NJ} = H;\ t^{m+1} = t^m + \tau,\ m = 0,1,\ldots\}$$

where τ is the time step. The grid was clustered near electrodes. Typical grids are shown in Fig. 4(a) and (b). A SOR by lines method with the Thomas algorithm was used for solution of the finite-difference equations. For each time step, several iterations were performed between equations for n_e, n_+, and φ. When these iterations were convergent, the voltage drop V is calculated on electrodes by the following formula, $V = E - IR_0$, where $I = \int_0^L en_e\mu_e E(x, y = H)\,dx$. After convergence of the internal iteration process, the computing procedure advances to the next time step. The process is repeated until the solution reaches a steady asymptote.

The characteristic time scales of the investigated phenomenon can be determined according to physical and mathematical statements of the problem. The following phenomena are taken into account: (a) the ionization of molecules N_2 by electronic impact, (b) the recombination of positively charged ions at collisions with electrons, (c) the drift of ions and electrons in an electric field, (d) the diffusion of charged particles and ambipolar diffusion, and (e) the relaxation of volumetric charge.

The characteristic times for the above listed processes are estimated for nitrogen. Drift velocities of electrons and ions in uniform electric field E are $V_{dr,e} = \mu_e E$ and $V_{dr,+} = \mu_+ E$. Previously, a characteristic

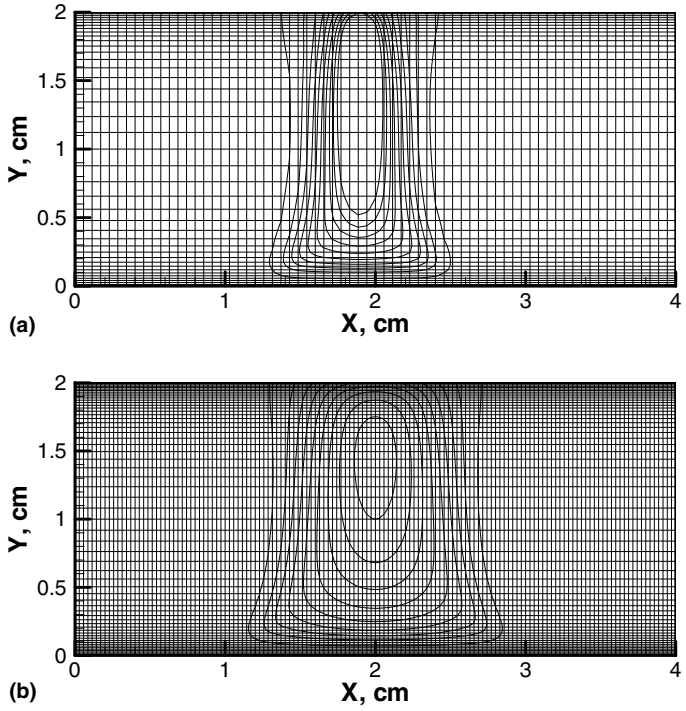

Fig. 4. (a) Computed contours of glow discharge on 71×41 grid. (b) Computed contour of glow discharge on 141×61 grid.

electric field has been described in the cathode layer and in the positive column of $E_{cl} = 4500$ V/cm, $E_{pc} = 100$ V/cm. Then, all drift velocities in the cathode layer and the positive column can be obtained for the present conditions ($p = 5$ torr) as $(V_{dr,e})_{cl} = 3.96 \times 10^8$ cm/s, $(V_{dr,+})_{cl} = 1.3 \times 10^6$ cm/s, $(V_{dr,e})_{pc} = 8.8 \times 10^6$ cm/s, $(V_{dr,+})_{pc} = 2.9 \times 10^4$ cm/s.

For the characteristic dimensions of this discharge field, it is possible to choose (a) the cathode layer $d_n = 0.1$ cm, (b) the positive column $H = 1$ cm. From these physical dimensions, the characteristic time scales of the drift motion are obtained as the following; $(t_{dr,e})_{cl} = 2.52 \times 10^{-10}$ s, $(t_{dr,+})_{cl} = 7.7 \times 10^{-8}$ s, $(t_{dr,e})_{pc} = 1.14 \times 10^{-7}$ s, and $(t_{dr,+})_{pc} = 3.45 \times 10^{-5}$ s.

The time of ionization can be estimated by the formula; $t_i = 1/\nu_i$ where $\nu_i = \nu_i(p)$ is the frequency of ionization. Frequency of ionization is connected to the drift velocity of electrons through Townsend's coefficient of ionization [3,7] $\nu_i = \alpha(E,p)V_{dr,e}$. The Townsend ionization coefficients at two values of electric field of $E_{cl} = 4500$ V/cm and $E_{pc} = 100$ V/cm are estimated to be $\alpha_{cl} \approx 41$ cm^{-1} and $\alpha_{pc} \approx 2.2 \times 10^{-6}$ cm^{-1}, respectively. From these values, the ionization frequency and the representative time scales of the ionization process are: $(\nu_i)_{cl} = 1.62 \times 10^{10}$ s^{-1}, $(t_i)_{cl} = 6.17 \times 10^{-11}$ s and $(\nu_i)_{pc} = 1.94 \times 10^1$ s^{-1}, $(t_i)_{pc} = 5.0 \times 10^{-2}$ s.

The recombination rate of charged particles can also be determined. A frequency of ion-electronic recombination is proportional to concentration of ions, $\nu_r = \beta n_+$, s^{-1}, therefore $t_r = 1/\beta n_+$, s. If one accepts that $\beta = 2 \times 10^{-7}$ cm^3/s and the concentration of ions is $(n_+)_{pc} = 5 \times 10^9$ cm^{-3}, then the typical time scale of the recombination of positively charged ions by collisions with electrons is $t_r \approx 10^{-3}$ s.

The time scales for the diffusion of charged particles and ambipolar diffusion can be assessed from the classic theory. An average square value of the displacement of any particle in diffusion process is given by Einstein's formula [3,7], $\langle x^2 \rangle = 2Dt$, where D is the diffusion coefficient, t is the time elapsed. Three types of charged particles diffusion are needed to be considered; (a) diffusion of electrons with $D_e = \mu_e T_e = 8.8 \times 10^4$ cm^2/s, (b) diffusion of ions with $D_+ = \mu_+ T_+ = 7.5$ cm^2/s, and (c) the ambipolar diffusion with diffusion coefficient $D_a = \mu_+ T_e = 290$ cm^2/s. Once the characteristic size $d_n = \Lambda = \sqrt{\langle x^2 \rangle} = 0.1$ cm is chosen, it yields $t_{dif,e} = \Lambda^2/2D_e = 5.68 \times 10^{-8}$ s, $t_{dif,+} = \Lambda^2/2D_+ = 6.67 \times 10^{-4}$ s, $t_{dif,a} = \Lambda^2/2D_a = 1.72 \times 10^{-5}$ s.

Finally, the characteristic relaxation time scale of the volumetric charge is estimated as follows. For a spatially homogeneous charge, the electrical density is defined by $\rho = e(n_+ - n_e)$. Then, the Gauss law required that $\mathrm{div}\mathbf{E} = 4\pi\rho = 4\pi e(n_+ - n_e) = \varepsilon(n_+ - n_e)$.

From the charge conservation equation $(\partial\rho/\partial t) + \mathrm{div}\,\mathbf{j} = 0$, where $\mathbf{j} = \sigma\mathbf{E}$, here it is assumed that total current is transferred by electrons, because of the great difference of mobility of electrons and ions. Thus, $(\partial\rho/\partial t) + \sigma\,\mathrm{div}\,\mathbf{E} + \mathbf{E}\,\mathrm{grad}\,\sigma = 0$. As we have assumed earlier, the charged particles distributed homogeneously, then $(\partial\rho/\partial t) + \sigma\,\mathrm{div}\,\mathbf{E} = (\partial\rho/\partial t) + 4\pi\sigma\rho = 0$, $\rho(t) = \rho(t=0)\exp(-4\pi\sigma t)$. The time scale of the volumetric charge relaxation, often referred to as the Maxwell's time, can be calculated by the formula [6,7], $t_M = 1/4\pi\sigma = 1/4\pi n_e \mu_e e = 1/\varepsilon n_e \mu_e$. Substituting all numerical values into this formula, it can be shown that the characteristic time for the relaxation of a volumetric charge is $t_M \approx 1.25 \times 10^{-9}$ s.

The stable and physically meaningful time step sizes for computations can now be analyzed. The dimensionless time τ, which appears in the system of Eq. (47) has the following expression $\tau = t(E\mu_e/H^2) = (t/t_0)$. The time scale $t_0 = (H^2/E\mu_e)$ has the following physical meaning; each electron needs this time for travelling through gas discharge gap under condition of uniform electric field $E_y = \bar{E} = E/H$. For typical values of Emf considered, (1) $E = 3000$ V, $\bar{E} = 1500$ V/cm and $t_0 = 1.52 \times 10^{-8}$ s, and (2) $E = 500$ V, $\bar{E} = 250$ V/cm and $t_0 = 9.09 \times 10^{-8}$ s.

It is apparent from the foregoing discussion that the investigated problem has a wide range of time scales. The fastest physical processes are ionization of molecules by electronic impact and drift of electrons in a cathode layer. The relaxation time of a volumetric charge has a scale 10^{-9} s. The characteristic time of ions drift in a cathode layer is proportional to 10^{-7} s. It means that to converge a solution in the cathode layer to its steady state asymptote, it is necessary to carry out calculations till the time elapse exceeded the value of 10^{-7} s, however, the calculation time step need not be shorter than $\sim 10^{-9}$ s.

Table 1
Representative time in seconds

	Cathode layer	Positive column
$t_{dr,e}$	2.52×10^{-10}	3.79×10^{-8}
$t_{dr,+}$	7.7×10^{-8}	1.15×10^{-5}
t_i	6.17×10^{-11}	1.87×10^{-7}
t_r	10^{-3}	
$t_{dif,e}$	5.68×10^{-8}	
$t_{dif,+}$	6.67×10^{-4}	
$t_{dif,a}$	1.72×10^{-5}	
t_m	1.25×10^{-9}	
t_0	1.52×10^{-8}	

The characteristic time of electrons drift in the positive column ($\sim 10^{-7}$ s) and ions drift in the positive column ($\sim 4.0 \times 10^{-5}$ s) is commensurable with electronic ($\sim 6.0 \times 10^{-8}$ s) and ambipolar diffusion ($\sim 2.0 \times 10^{-5}$ s). The diffusion time of ions ($\sim 7.0 \times 10^{-4}$ s) is compatible with representative recombination time ($\sim 10^{-3}$ s). As all the listed processes can render appreciable influence on a physically meaningful steady state solution under those constraints, it is assumed that the range of time scales vary greatly through the values from 10^{-11} to 10^{-3} s. It is obvious; the required temporal resolution of the present problem imposes a significant computing challenge.

The adopted finite difference method allows calculations with time steps that cannot be compatible with all the time scales considered in here. It is well known that the computational stability of any calculations is determined by the type of equations to be solved, finite-difference approximation method, and quality of grids [17,18]. However, it is possible to specify two dimensionless criteria of computational stability to guide the selection of the allowable time step. The Courant–Friedrichs–Lewy (CFL) numbers for convection and diffusion are $\mathrm{CFL}_h = a\Delta t/h \sim 1$, $\mathrm{CFL}_p = (2D\Delta t/h^2) \sim 1$, where a is the characteristic value of velocity, Eq. (47), Δt is the time step and h is the spatial spacing of the grid.

The fact that CFL numbers are limited to unit does not mean that these conditions are neither optimal nor necessary for the present numerical simulation. These criteria are dictated by the stability condition of explicit finite-difference schemes for the linear transfer model equations with dissipation. By examining Eq. (47), it reveals that there is a scale of speed $\tilde{V} = \mu_e E/H$ which corresponds to the electrons drift velocity in a uniform electric field with intensity $E_y = E/H$. For a typical calculation with E = 3000 V and $H = 2$ cm, it was found $\tilde{V} = 1,32 \times 10^8$ cm/s. If an explicit finite-difference scheme is used for solving of Eq. (47), the limiting time steps are dictated by the CFL condition. For the present investigation, $a = (V_{dr,e})_{cl} = 3.96 \times 10^8$ cm/s, $h = 0.1 d_n = 0.01$ cm, $\Delta t_h = h/a = 2.53 \times 10^{-11}$ cm/s, and $\Delta t_p = h^2/2D = 5.68 \times 10^{-10}$ cm/s. The dimensionless time step should be $\tau = ((\min(\Delta t_h, \Delta t_p))/t_0) = 1.66 \times 10^{-3}$.

Summary of the characteristic time scales for glow discharge in N_2 at $p = 5$ torr, $E = 3$ kV is given in Table 1.

7. Computing accuracy assessment

As it has been shown in reference [17], the present finite difference scheme for solving Eq. (47) is formally second order accurate for a smooth solution. However, in the region of steep gradients, the accuracy of this scheme deteriorates to a first-order approximation. Therefore, it is necessary to assess the effect of numerical dissipation to the overall accuracy of the solution. In the present analysis, an attempt has been made to compare the numerical dissipation with physical diffusion, or numerical diffusion fluxes with physical drift and diffusion fluxes for the first order finite-difference equation.

$$\frac{u_i^{m+1}-u_i^m}{\tau}+a\frac{u_i^m-u_{i-1}^m}{h}=0,\quad u_i^{m=0}=u_i(t=0,x_i)=\varphi_i(x_i).$$

For the model linear convection equation

$$\frac{\partial u}{\partial t}+a\frac{\partial u}{\partial x}=0,\quad a>0,\quad u(t=0,x)=\varphi_0(x).$$

One can show that the above finite-difference approximation is equivalent to the following differential equation:

$$\frac{\partial u}{\partial t}+a\frac{\partial u}{\partial x}=D_{\mathrm{n}}\frac{\partial^2 u}{\partial x^2},\quad \text{where } D_{\mathrm{n}}=\frac{ah}{2}\left(1-\frac{a\tau}{h}\right)=\frac{ah}{2}(1-\mathrm{CFL}_h)$$

and D_{n} is the numerical diffusion coefficient. It means that upper bound of the numerical diffusion coefficient is $D_{\mathrm{n}}=ah/2$.

The representative diffusion and drift fluxes have been determined previously for a typical glow discharge. The numerical diffusion fluxes for electrons and ions in the y-direction are (formulas for numerical diffusion fluxes in the x-direction are analogous):

$$(\Gamma_{\mathrm{e,n}})_y=-D_{\mathrm{e,n}}\frac{\partial n_{\mathrm{e}}}{\partial y},\quad (\Gamma_{+,\mathrm{n}})_y=-D_{+,\mathrm{n}}\frac{\partial n_+}{\partial y},$$

where $D_{\mathrm{e,n}}=0.5\Delta y\cdot V_{\mathrm{e,dr}}$, $D_{+,\mathrm{n}}=0.5\Delta y\cdot V_{+,\mathrm{dr}}$ or $D_{\mathrm{e,n}}=0.5\Delta y\cdot\mu_{\mathrm{e}}(\partial\varphi/\partial y)$, $D_{+,\mathrm{n}}=0.5\Delta y\cdot\mu_+(\partial\varphi/\partial y)$. Assume $\partial\varphi/\partial y\approx\Delta\varphi/\Delta y$, it is then obtained $D_{\mathrm{e,n}}\approx(\mu_{\mathrm{e}}\Delta\varphi)/2$, $D_{+,\mathrm{n}}\approx(\mu_+\Delta\varphi)/2$, and $(\Gamma_{\mathrm{e,n}})_y\approx 0.5\mu_{\mathrm{e}}\Delta\varphi((\Delta n_{\mathrm{e}})/(\Delta y))$, $(\Gamma_{+,\mathrm{n}})_y\approx 0.5\mu_+\Delta\varphi((\Delta n_+)/(\Delta y))$.

Since coefficients of physical diffusion are determined by Einstein's formulas, the relations between physical diffusion and numerical diffusion fluxes are:

$$\frac{\Gamma_{\mathrm{e,dif}}}{\Gamma_{\mathrm{e,n}}}\approx\frac{2T_{\mathrm{e}}}{\Delta\varphi},\quad \frac{\Gamma_{+,\mathrm{dif}}}{\Gamma_{+,\mathrm{n}}}\approx\frac{2T_+}{\Delta\varphi}.$$

The corresponding relations between physical drift fluxes and numerical diffusion fluxes become:

$$\frac{\Gamma_{\mathrm{e,dr}}}{\Gamma_{\mathrm{e,n}}}\approx 2\frac{n_{\mathrm{e}}}{\Delta n_{\mathrm{e}}},\quad \frac{\Gamma_{+,\mathrm{dr}}}{\Gamma_{+,\mathrm{n}}}\approx 2\frac{n_+}{\Delta n_+}.$$

So, one can conclude that for the calculation on a typical grid, for example 100×100,

$$\Gamma_{\mathrm{e,dr}}\gg\Gamma_{\mathrm{e,n}}\sim\Gamma_{\mathrm{e,dif}},\quad \Gamma_{+,\mathrm{dr}}\gg\Gamma_{+,\mathrm{n}}\gg\Gamma_{+,\mathrm{dif}}.$$

These results show that on a coarse grid the physical drift fluxes can be on the same order of magnitude as that of the numerical diffusion fluxes in the cathode layer.

8. Numerical results

The glow discharge in nitrogen is investigated between flat plate electrodes of 4 cm in length and 2 cm apart. The discharge is maintained by an electric field of the range from 1 to 2 kV, ($1<E<2$ kV), the external circuit has a resistance of 300 kΩ, and the ambient pressure ranges from 5 to 10 torr. The applied transverse magnetic field is limited to a maximum magnitude of 0.1 T ($-0.1<B<0.1$). For all numerical simulations, the coefficient of the secondary electronic emission is assumed to have the range from 0.1 to 0.3 [7].

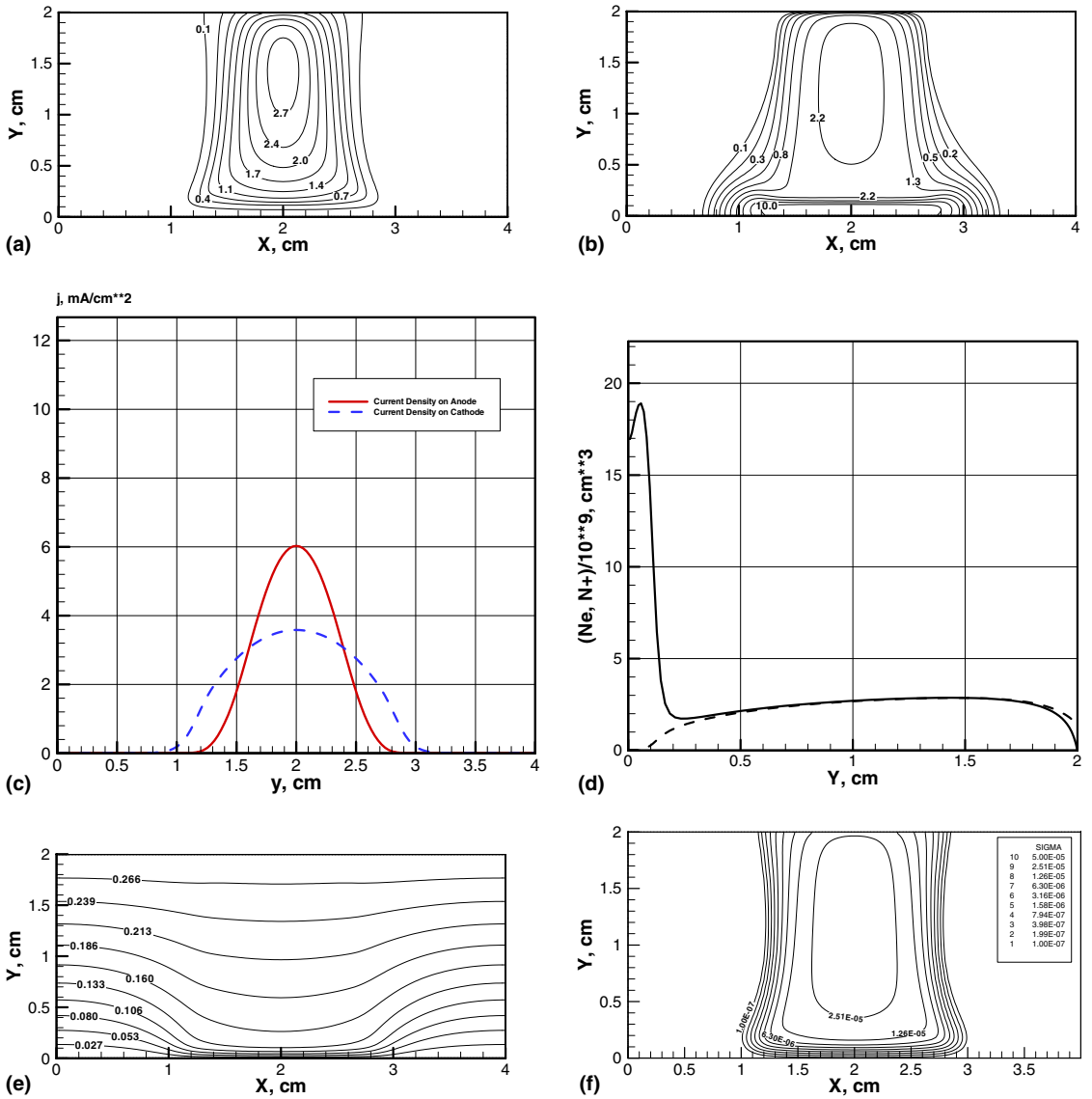

Fig. 5. (a) Electron contours in the gas discharge gap at $p = 5$ torr, $E = 2$ kV, $\gamma = 0.1$, $H = 2$ cm; $I = 4.85$ mA, $j_{c,max} = 3.58$ mA/cm^2, $j_{a,max} = 6.03$ mA/cm^2, $V = 533$ V; The concentration levels are normalized by the value of cm^3. Parameters of the one-dimensional normal glow discharge (the Engel–Steenbeck theory): cm, V, mA/cm^2. (b) Ion contours in the gas discharge gap at $p = 5$ torr, $E = 2$ kV, $\gamma = 0.1$, $H = 2$ cm; $I = 4.85$ mA, $j_{c,max} = 3.58$ mA/cm^2, $j_{a,max} = 6.03$ mA/cm^2, $V = 533$ V; The concentration levels are normalized by the value $N_0 = 10^{-9}$ cm^{-3}. Parameters of the one-dimensional normal glow discharge (the Engel–Steenbeck theory): $d_n = 0.15$ cm, $V_n = 205$ V, $J_n = 1.37$ mA/cm^2. (c) Current density on the anode (solid line) and cathode (dashed line); $p = 5$ torr, $E = 2$ kV, $\gamma = 0.1$, $H = 2$ cm; $I = 4.85$ mA, $j_{c,max} = 3.58$ mA/cm^2, $j_{a,max} = 6.03$ mA/cm^2, $V = 533$ V. Parameters of the one-dimensional normal glow discharge (the Engel–Steenbeck theory): $d_n = 0.15$ cm, $V_n = 205$ V, $J_n = 1.37$ mA/cm^2. (d) Distribution of electron (dashed line) and ion (solid line) concentrations along the glow discharge centerline; $p = 5$ torr, $E = 2$ kV, $\gamma = 0.1$, $H = 2$ cm; $I = 4.85$ mA, $j_{c,max} = 3.58$ mA/cm^2, $j_{a,max} = 6.03$ mA/cm^2, $V = 533$ V. (e) Electrical potential at $p = 5$ torr, $E = 2$ kV, $\gamma = 0.1$, $H = 2$ cm; $I = 4.85$ mA, $j_{c,max} = 3.58$ mA/cm^2, $j_{a,max} = 6.03$ mA/cm^2, $V = 533$ V; Numbers on curves are φ/E. (f) Electrical conductivity (Ω^{-1} cm^{-1}) contours in the gas discharge gap at $p = 5$ torr, $E = 2$ kV, $\gamma = 0.1$, $H = 2$ cm; $I = 4.85$ mA, $j_{c,max} = 3.58$ mA/cm^2, $J_{a,max} = 6.03$ mA/cm^2, $V = 533$ V.

The influence of the secondary electronic emission coefficient γ on the glow discharge structure was also investigated. As it has been mentioned earlier, this coefficient is characterized by the electrical property of electrode material. In addition, this coefficient strongly depends on the intensity of the near-cathode electric field. Unfortunately, the nature of this dependency is still not satisfactorily understood, therefore the constant values of γ are applied to all present calculations.

Numerical results obtained for different pressures p, Emf of power supply E, and γ were compared with the classical theory of Engel and Steenbeck [3,4]. This theory gives the classic results for the cathode voltage drop V_n, the depth of the cathode layer $(pd)_n$ and the normal current density j_n, see Eqs. (54)–(56).

It should be stressed that the Engel and Steenbeck theory [3] is an approximate theory of the normal glow discharge for the one-dimensional cathode layer. At the same time, many experimental and theoretical studies have substantiated these predictions, which give the credence to their theory for glow discharges. Therefore, the comparison with this theory is chosen as validation base for the present calculations. The normal current densities predicted by the Engel and Steenbeck theory (j_n) are presented in legends for numerical simulation results. These legends also contain values of total current I, the maximum values of current density on cathode $(j_{c,max})$ and anode $(j_{a,max})$, as well as the total voltage drop V across the gas discharge gap.

The investigated glow discharge exists in the mode of ''normal density current'', where the current column occupies only a part of the gas discharge space [6]. Based on the current density distribution along the cathode, one can conclude that boundary effects (diffusion and drift in the x-direction) are significant. It means that current density in the case under consideration must exceed the predicted value by the idealized theory of Engel and Steenbeck [3,4]. In conformity with this understanding, the ''normal current density'', which is obtained from the one-dimensional theory of Engel and Steenbeck, is $j_n = 1.37$ mA/ cm^2.

A glow discharge at $p = 5$ torr, $E = 2$ kV, $\gamma = 0.1$ of the basic configuration is shown in Fig. 5. Initial conditions for these calculations correspond to the glow discharge without an externally applied magnetic field. The basic elements of the glow discharge structure are simulated by the present computing model. The area of charged space near cathode is confined to a very small dimension along the y-axis. In this case the height of the cathode layer has the value of $\sim$0.15 cm, that agrees very well with value 0.151 cm, which is predicted by the one-dimensional theory of Engel and Steenbeck. However, it should be noted that uncertainty in the determination of d_n from the numerical results is understandable.

Two-dimensional distributions of electron and ion concentrations are shown in Fig. 5(a) and (b). In the present results, the levels of concentration are normalized by the value of $N_0 = 10^9$ cm^{-3} for the glow discharge. It is particularly interesting to note that the extremely high ion concentration is located immediately adjacent to the cathode. This phenomenon has been frequently observed in experiments and a greater value of nearly one order of magnitude is indicated by the present calculation.

The current densities on the cathode and anode are shown in Fig. 5(c). Distributions of electron and ion concentrations along y-axis are shown in Fig. 5(d). In the last figure, one can clearly define the main domains of glow discharge; (1) the area of positive charge space near to cathode (the cathode layer), (2) the area of negative charge space near to anode (the anode layer), and (3) the area of a quasineutral plasma (the positive column).

In Fig. 5(d), the computed electron and ion number densities exhibit the anticipated electric neutrality of the glow discharge path away from the sheath region. The cathode fall is also duplicated by the calculated electric potential in Fig. 5(e). Finally, the electric conductivity of the glow discharge based on the computed electron mobility is depicted in Fig. 5(f) to show the previously unobtainable detailed variation of the glow discharge. This value was calculated by the following formula, $\sigma_e = e\mu_e n_e$. It should be stressed that in the case with external magnetic field the electrical conductivity becomes a tensor, $\sigma_\parallel = \sigma_e + (1/(1 + b_e^2))$, $\sigma_\perp = \sigma(b_e/(1 + b_e^2))$, where $\sigma_\parallel$, $\sigma_\perp$ are the electrical conductivities in the parallel and perpendicular orientations of the applied external magnetic field, respectively [7,8].

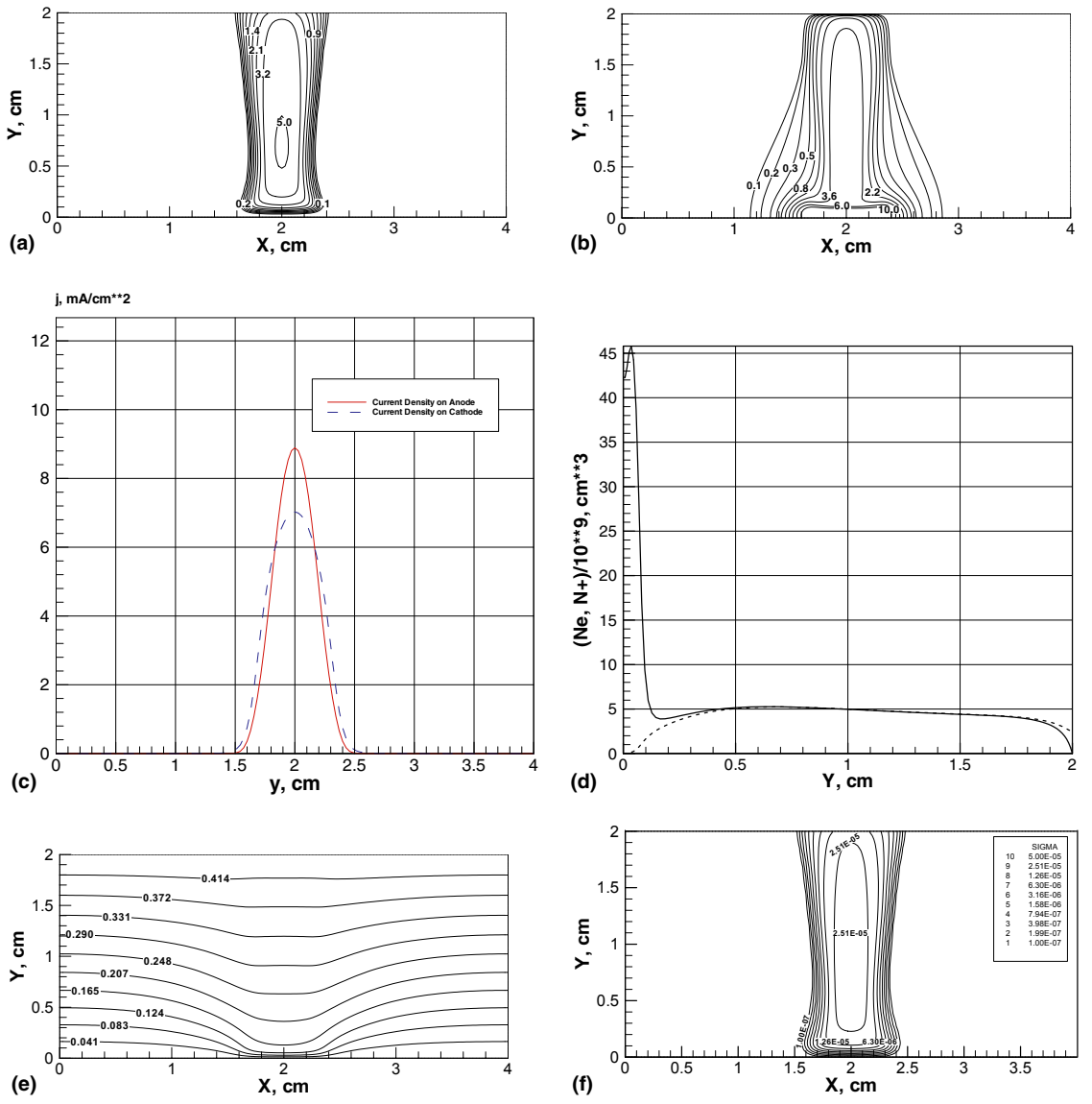

Fig. 6. (a) Electron contours in the gas discharge gap at $p = 10$ torr, $E = 2$ kV, $\gamma = 0.1$, $H = 2$ cm; $I = 3.9$ mA, $j_{c,max} = 7.03$ mA/cm^2, $j_{a,max} = 8.89$ mA/cm^2, $V = 835$ V. The concentration levels are normalized by the value of $N_0 = 10^{-9}$ cm^{-3}. Parameters of the one-dimensional normal glow discharge (the Engel–Steenbeck theory): $d_n = 0.0755$ cm, $V_n = 205$ V, $j_n = 5.49$ mA/cm^2. (b) Ion contours in the gas discharge gap at $p = 10$ torr, $E = 2$ kV, $\gamma = 0.1$, $H = 2$ cm; $I = 3.9$ mA, $j_{c,max} = 7.03$ mA/cm^2, $j_{a,max} = 8.89$ mA/cm^2, $V = 835$ V. The concentration levels are normalized by the value of $N_0 = 10^{-9}$ cm^{-3}. Parameters of the one-dimensional normal glow discharge (the Engel–Steenbeck theory): $d_n = 0.0755$ cm, $V_n = 205$ V, $j_n = 5.49$ mA cm^2. (c) Current density on the anode (solid line) and cathode (dashed line); $p = 10$ torr, $E = 2$ kV, $\gamma = 0.1$, $H = 2$ cm; $I = 3.9$ mA, $j_{c,max} = 7.03$ mA/cm^2, $j_{a,max} = 8.89$ mA/cm^2, $V = 835$ V; Parameters of the one-dimensional normal glow discharge (the Engel–Steenbeck theory): $d_n = 0.0755$ cm, $V_n = 205$ V, $j_n = 5.49$ mA/cm^2. (d) Distribution of electron (dashed line) and ion (solid line) concentrations along the glow discharge centerline; $p = 10$ torr, $E = 2$ kV, $\gamma = 0.1$, $H = 2$ cm; $I = 3.9$ mA, $j_{c,max} = 7.03$ mA/cm^2, $j_{a,max} = 8.89$ mA/cm^2, $V = 835$ V. (e)Electrical potential $p = 10$ torr, $E = 2$ kV, $\gamma = 0.1$, $H = 2$ cm; $I = 3.9$ mA, $j_{c,max} = 7.03$ mA/cm^2, $j_{a,max} = 8.89$ mA/cm^2, $V = 835$ V; numbers on curves are φ/E. (f) Electrical conductivity ($Omega^{-1}$ cm^{-1}) contours in the gas discharge gap at $p = 10$ torr, $E = 2$ kV, $\gamma = 0.1$, $H = 2$ cm; $I = 3.9$ mA, $j_{c,max} = 7.03$ mA/cm^2, $J_{a,max} = 8.89$ mA/cm^2, $V = 835$ V.

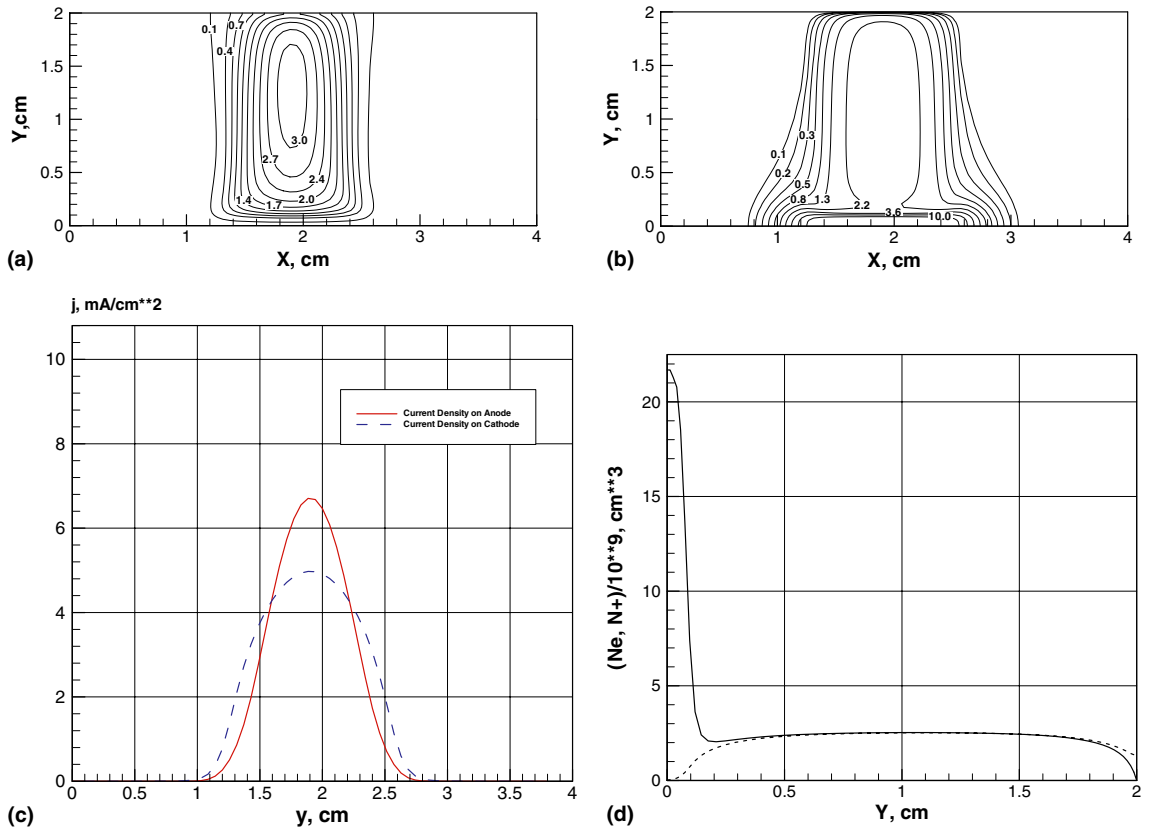

Fig. 7. (a) Electron contours in the gas discharge gap at $p = 5$ torr, $E = 2$ kV, $\gamma = 0.3$, $H = 2$ cm; $I = 4.85$ mA, $j_{c,max} = 4.97$ mA/cm^2, $j_{a,max} = 6.7$ mA/cm^2, $V = 454$ V; The concentration levels are normalized by the value of $N_0 = 10^{-9}$ cm^{-3}; Parameters of the one-dimensional normal glow discharge (the Engel–Steenbeck theory): $d_n = 0.0924$ cm, $V_n = 125$ V, $j_n = 2.65$ mA/cm^2. (b) Ion contours in the gas discharge gap at $p = 5$ torr, $E = 2$ kV, $\gamma = 0.3$, $H = 2$ cm; $I = 4.85$ mA, $j_{c,max} = 4.97$ mA/cm^2, $j_{a,max} = 6.7$ mA/cm^2, $V = 454$ V; The concentration levels are normalized by the value of $N_0 = 10^{-9}$ cm^{-3}; Parameters of the one-dimensional normal glow discharge (the Engel–Steenbeck theory): $d_n = 0.0924$ cm, $V_n = 125$ V, $j_n = 2.65$ mA/cm^2. (c) Current density on the anode (solid line) and cathode (dashed line); $p = 5$ torr, $E = 2$ kV, $\gamma = 0.3$, $H = 2$ cm; $I = 4.85$ mA, $j_{c,max} = 4.97$ mA/cm^2, $j_{a,max} = 6.7$ mA/cm^2, $V = 454$ V; Parameters of the one-dimensional normal glow discharge (the Engel–Steenbeck theory): $d_n = 0.0924$ cm, $V_n = 125$ V, $j_n = 2.65$ mA/cm^2. (d) Distribution of electron (dashed line) and ion (solid line) concentrations along the glow discharge centerline; $p = 5$ torr, $E = 2$ kV, $\gamma = 0.3$, $H = 2$ cm; $I = 4.85$ mA, $j_{c,max} = 4.97$ mA/cm^2, $j_{a,max} = 6.7$ mA/cm^2, $V = 454$ V.

The data presented in Fig. 5 will be used further for comparison with other computing simulations. To investigate the influence of different input parameters on the gas discharge structure, additional numerical experiments were performed. First of all, numerical simulations have been performed to study the influence of gas pressure and Emf of power supply on electrodynamic structure of the glow discharge. The influence of external magnetic field on the glow discharge structure was also performed for different gas pressure in the range from 5 to 10 torr.

The glow discharge behavior, by increasing the Emf of external circuits, results in the increasing of transversal (along x-axes) size of the positive column which is faithfully reproduced. At the same time, the transverse discharge space size adjacent to the cathode is also substantially greater. This tendency is repeated for all investigated pressures ($p = 5$, 10 torr) and for other coefficients of the secondary electron emission. Actually, the different electron emission coefficients have really simulated different types of the cathode materials; $\gamma = 0.1$–0.3.

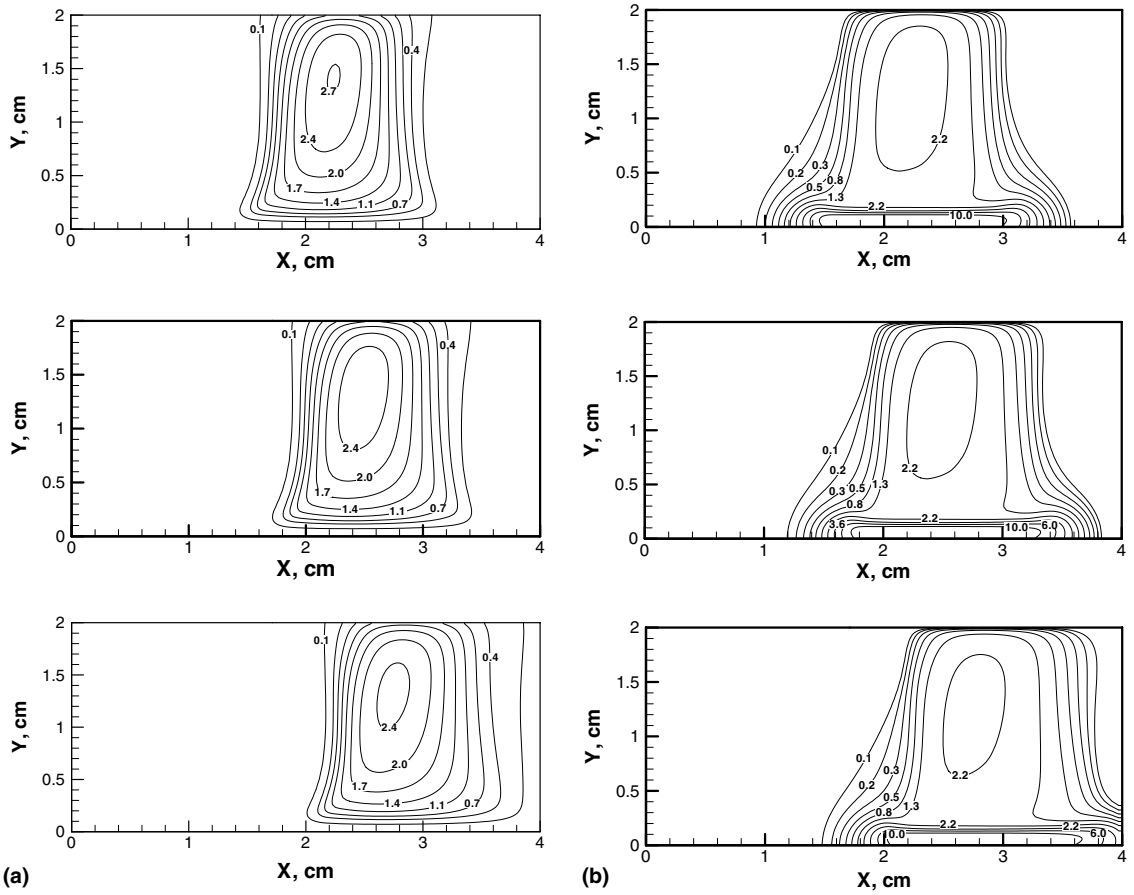

Fig. 8. (a) Electron contours (in 10^9 cm^{-3}) in the gas discharge gap at time moments $t = 50$, 100, 150 μs; $p = 5$ torr, $E = 2$ kV, $\gamma = 0.1$, $H = 2$ cm, $B = 0.01$ T. (b) Ion contours (in 10^9 cm^{-3}) in the gas discharge gap at time moments $t = 50$, 100, 150 μs; $p = 5$ torr, $E = 2$ kV, $\gamma = 0.1$, $H = 2$ cm, $B = 0.01$ T.

Decreasing the gas discharge pressure results in a considerable increase not only in the width of the discharge, but also the thickness of the cathode layer. This observation is in full accordance with the Engel and Steenbeck theory [3,4]. The reverse behavior is also confirmed by the present numerical results; by increasing the ambient pressure all characteristic sizes of a glow discharge are decreased.

Computed results of the glow discharge at $p = 10$ torr and $E = 2$ kV are shown from Fig. 6(a)–(f). As in the earlier presentation, these figures present the electron (a) and ion (b) concentrations, the current density distribution along the cathode and anode (c), distributions of electron and ion concentrations of the glow discharge along the centerline in the y-direction (d), electrical potential (e), and contours of electrical conductivity (f). The corresponding theoretical result of the Engel and Steenbeck theory is obtained for the case of the following parameters: $d_n = 0.0755$ cm, $V_n = 205$ V, $j_n = 5.49$ mA/cm^2. These values are in good agreement with the present numerical results.

By comparing spatial distributions of the electrical conductivity at pressures $p = 5$ torr (Fig. 5(f)) and $p = 10$ torr (Fig. 6(f)), one can detect a decreasing degree of ionization which is in perfect accordance with the laws of nature. It is a well-known consequence; at the higher pressure a higher collisional frequency of

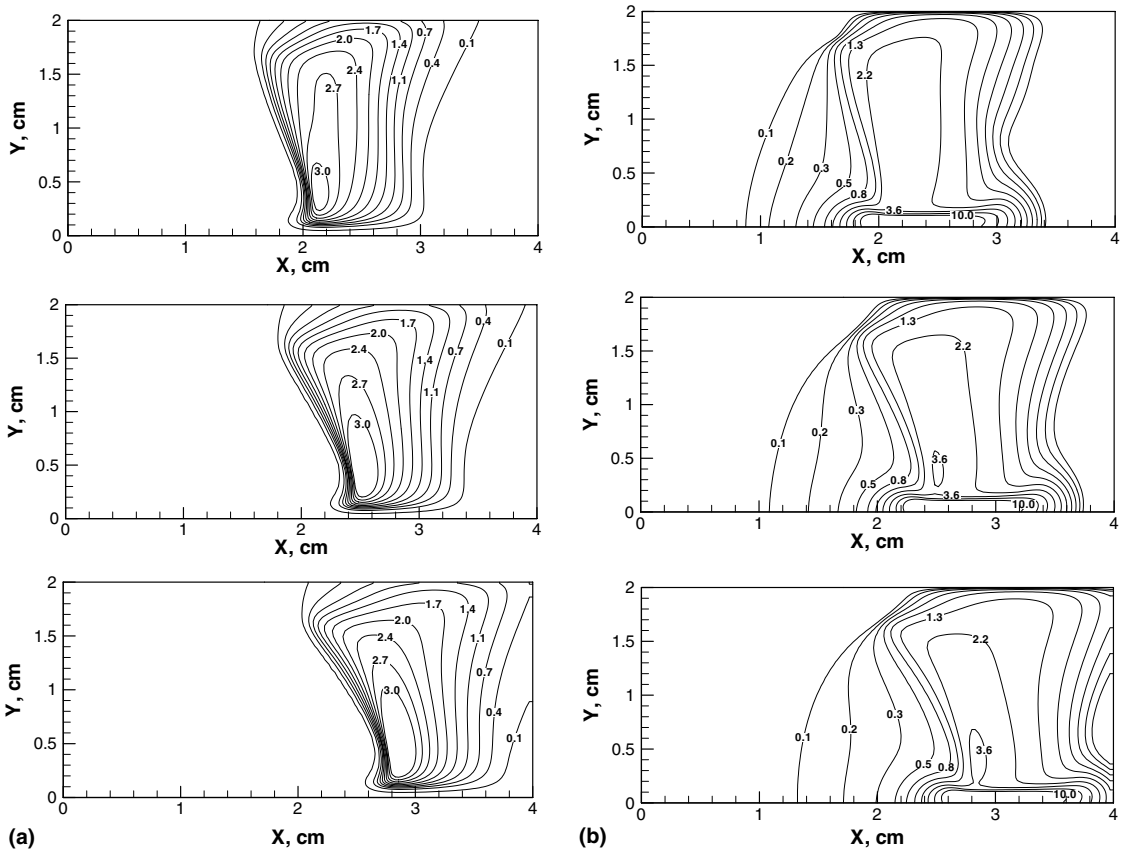

Fig. 9. (a) Electron contours (in 10^9 cm^{-3}) in the gas discharge gap at time moments $t = 10$, 20, 30 μs; $p = 5$ torr, $E = 2$ kV, $\gamma = 0.1$, $H = 2$ cm, $B = 0.05$ T. (b) Ion contours (in 10^9 cm^{-3}) in the gas discharge gap at time moments $t = 10$, 20, 30 ms; $p = 5$ torr, $E = 2$ kV, $\gamma = 0.1$, $H = 2$ cm, $B = 0.05$ T.

electrons with neutral particles will take place [6]. Therefore, to ionize similar volumes of neutral gas, a higher level of voltage drop across a gas discharge gap is required. In the present calculation, moderate increase in the value of the voltage drop (compare: $V = 835$ V at $p = 10$ torr and $V = 533$ V at $p = 5$ torr) still produces a decreased volume of the gas discharge.

As it has been discussed previously, the secondary electronic emission coefficient γ is a very significant input parameter of the developed model, which simulates different electrode materials. Fig. 7(a)–(d) show parameters of the glow discharge at $\gamma = 0.3, p = 5$ torr, $E = 2$ kV. Even from the presented results, one can see significant changes in the glow discharge structure. For the cases investigated, the depth of the cathode layer and transverse size of the cathode spot are decreasing in accordance with the Engel andSteenbeck theory $d_n = 0.0924$ cm, $V_n = 125$ V, $j_n = 2.65$ mA/cm^2). In short, the present results capture all essential features of glow discharge physics and are validated by the classic theory by von Engel and Steenbeck [3,4]. Additional direct comparison with experimental data is planned for the future.

From the theory developed in the present work, a transverse magnetic field will affect the gas discharge structure at $b_e \sim 1$ (and, especially at $b_i \sim 1$). It was found that the inductivity of the magnetic field exerts influence on the global structure of the glow discharge. Figs. 8 and 9 show electron and ion contours in the glow discharge at $p = 5$ torr and $E = 2$ kV at consecutive instants after magnetic field of $B = +0.01$ T

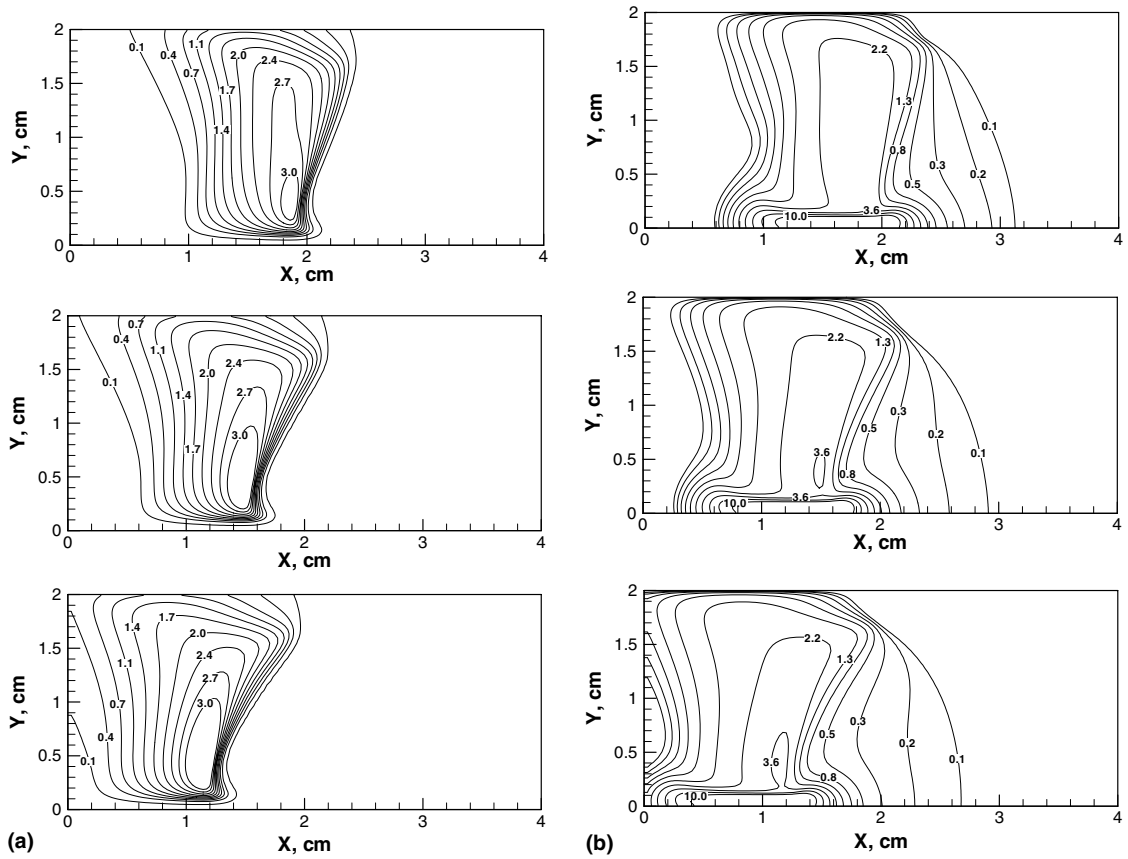

Fig. 10. (a) Electron contours (in 10^9 cm^{-3}) in the gas discharge gap at time moments $t = 10$, 20, 30 ms; $p = 5$ torr, $E = 2$ kV, $\gamma = 0.1$, $H = 2$ cm, $B = -0.05$ T. (b) Ion contours (in 10^9 cm^{-3}) in the gas discharge gap at time moments $t = 10$, 20, 30 ms; $p = 5$ torr, $E = 2$ kV, $\gamma = 0.1$, $H = 2$ cm, $B = 0.05$ T.

(Fig. 8) and $B = +0.05$ T (Fig. 9) is applied, respectively. These are transient configurations of the direct glow discharge.

In all cases presented, the discharge column moves continuously along electrode surfaces. First of all, it is revealed that a transverse magnetic field shifts discharge path from the initial position. Comparing numerical simulations for different magnetic fields B (Figs. 8 and 9), one can conclude that velocity of the discharge drifts perpendicular to applied magnetic field and is proportional to the value of B. The average velocity of such drift in the first case ($B = +0.01$ T) equals to $V_{B,\mathrm{drift}} \approx 6.5 \times 10^3$ cm/s, and in the second case ($B = +0.05$ T) $-V_{B,\mathrm{drift}} \approx 3.5 \times 10^4$ cm/s. Due to the nature of ambipolar mechanism, these drift velocities are much less than electronic drift velocities but greater than the ionic drift velocities.

The direction of shift depends upon the polarity of the applied magnetic field. Fig. 10(a) and (b) show distributions of electron and ion concentrations at the same successive instants as they have been shown in Fig. 9(a) and (b), but at a magnetic field of $B = -0.05$ T. Reversing the magnetic field polarity results in a corresponding shift of ions and electrons distributions relative to the center-plane of the discharge (compare Figs. 9 and 10).

Fig. 11 shows electron and ion contours in the glow discharge at $p = 10$ torr and $E = 2$ kV at consecutive instants ($t = 10$, 20 and 30 μs) after a magnetic field of $B = +0.1$ T is applied. This calculation, however, is

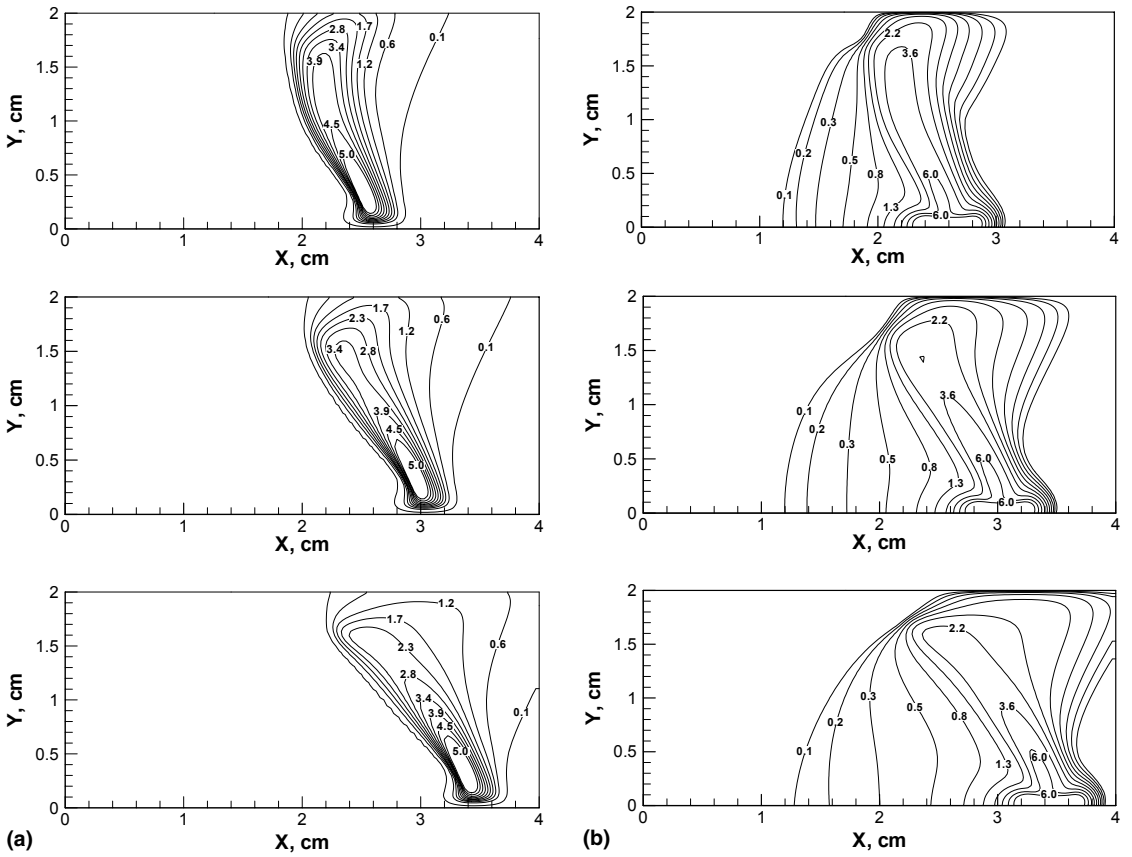

Fig. 11. (a) Electron contours (in 10^9 cm^{-3}) in the gas discharge gap at time moments $t = 10$, 20, 30 ms; $p = 10$ torr, $E = 2$ kV, $\gamma = 0.1$, $H = 2$ cm, $B = 0.1$ T. (b) Ion contours (in 10^9 cm^{-3}) in the gas discharge gap at time moments $t = 10$, 20, 30 ms; $p = 10$ torr, $E = 2$ kV, $\gamma = 0.1$, $H = 2$ cm, $B = 0.1$ T.

obtained under a higher ambient pressure ($p = 10$ torr). Therefore, to achieve the same drift velocity of the discharge plasma in magnetic field as that of the previous calculation ($p = 5$ torr and $B = +0.05$ T; Fig. 9), there is a need to apply a stronger magnetic field.

9. Conclusions

A theory and two-dimensional numerical simulations for modeling the electrodynamic structure of the glow discharges with magnetic field are presented. Two different physical-based boundary conditions are derived to extend the applicable range of the drift-diffusion glow discharge into the plasma sheath region. The drift-diffusion model with modified numerical boundary conditions has successfully simulated the complete glow discharge physics including the sheath regions.

All two-dimensional calculations of the glow discharge structure in nitrogen have been performed under various initial values and boundary conditions. The computed results exhibit good agreement with the classic theory of von Engel and Steenbeck.

The present result also demonstrated a new capability to simulate numerically the influence of a strong and a physically reasonable external magnetic field to a gas discharge structure.

References

[1] E.L. Resler, W.R. Sears, The prospects for magneto-aerodynamics, J. AeroSci. 25 (1958) 45–235, 258.
[2] J.S. Shang, Recent research in magneto-aerodynamics, Progr. Aerosp. Sci. 37 (2001) 1–20.
[3] A. von Engel, M. Steenbeck, Elektrische Gasentladungen, vol. II, Springer, Berlin, 1932.
[4] A. von Engel, Ionized Gases, Clarendon Press, Oxford, 1955.
[5] S.C. Brown, Introduction to Electrical Discharges in Gases, Wiley, New York, 1966.
[6] A.M. Howatson, An Introduction to Gas Discharge, second ed., Pergamon Press, Oxford, 1975 (first ed., 1965).
[7] Yu.P. Raizer, Gas Discharge Physics, Springer, New York, 1991.
[8] M. Mitchner, C.H. Kruger Jr., Partially Ionized Gases, Wiley-Interscience, New York, 1992.
[9] A.L. Ward, Effect of space charge in cold-cathode gas discharges, Phys. Rev. 112 (6) (1958) 1852–1857.
[10] A.L. Ward, Calculations of cathode-fall characteristics, J. Appl. Phys. 33 (9) (1962) 2789–2794.
[11] D.B. Graves, K.E.A. Jensen, Continuum model of DC and RF discharges, IEEE Trans. Plasma Sci. V.PS-14 (2) (1986) 78–91.
[12] J.P. Boeuf, E. Marode, A Monte Carlo analysis of an electron swarm in a non-uniform field: the cathode region of a glow discharge in helium, J. Phys. D 12 (1982) P2169–P2187.
[13] Yu.P. Raizer, S.T. Surzhikov, Two-dimensional structure of the normal glow discharge and the role of diffusion in forming of cathode and anode current spots, High Temp. 26 (3) (1988).
[14] Yu.P. Raizer, S.T. Surzhikov, Diffusion of charges along current and effective numerical method of eliminating of numerical dissipation at calculations of glow discharge, High Temp. 28 (3) (1990).
[15] I.P. Shkarofsky, T.W. Johnston, M.P. Bachynski, The Particle Kinetics of Plasmas, Addison-Wesley, Reading, MA, 1966.
[16] J.S. Shang, Shared knowledge in computational fluid dynamics, electromagnetics, and magneto-aerodynamics, Progr. Aerosp. Sci. 38 (2002) 449–469.
[17] R.D. Richtmyer, K.W. Morton, Difference Methods for Initial-Value Problems, Wiley, New York, 1967.
[18] J.C. Tanehill, D.A. Anderson, R.H. Pletcher, Computational Fluid Mechanics and Heat Transfer, second ed., Taylor & Francis, Washington, 1997.